

J R C T E C H N I C A L R E P O R T S

External quality control of Pléiades orthoimagery

Part I: Geometric benchmarking and validation of
Pléiades-1A orthorectified
data acquired over Maussane
test site

J. Grazzini
S. Lemajic
P. Astrand

2013

Report EUR 26101 EN

European Commission
Joint Research Centre
Institute for Environment and Sustainability

Contact information

P. Astrand
Address: Joint Research Centre, Via Enrico Fermi 2749, TP 266, 21027 Ispra (VA), Italy
E-mail: par-johan.astrand@jrc.ec.europa.eu
Tel.: +39 0332 78 6215
Fax: +39 0332 78 6325

<http://cidportal.jrc.ec.europa.eu/> <http://www.jrc.ec.europa.eu/>

This publication is a Reference Report by the Joint Research Centre of the European Commission.

Legal Notice

Neither the European Commission nor any person acting on behalf of the Commission is responsible for the use which might be made of this publication.

Europe Direct is a service to help you find answers to your questions about the European Union
Freephone number (*): 00 800 6 7 8 9 10 11
(*) Certain mobile telephone operators do not allow access to 00 800 numbers or these calls may be billed.

A great deal of additional information on the European Union is available on the Internet.
It can be accessed through the Europa server <http://europa.eu/>.

JRC82308

EUR 26101 EN

ISBN 978-92-79-32538-0

Contents

Abstract	ii
Acknowledgments	iii
1 Introduction.....	4
1.1 Objectives.....	4
1.2 Context.....	5
2 Píeiades sensor	6
3 Benchmarking methodology.....	8
3.1 Test cases definition	8
3.2 Test workflow design.....	11
4 Input data	11
4.1 Maussane test site and primary images	12
4.2 Ancillary data: DEM and CPs.....	14
4.3 Known issues on ancillary data.....	15
5 Orthorectification process	17
5.1 Ancillary modeling data preparation.....	18
5.2 Ortho data production.....	20
5.3 Known issues on the orthorectification process	21
6 External geometric quality control.....	23
6.1 Auxiliary validating data preparation	23

6.2 Error measurement	25
6.3 Overall results	27
7 Conclusion	34
Annexes	35
A.1 Image quality control and assurance.....	35
A.2 Orthoimage technical specifications for the purpose of LPIS	36
A.3 Additional primary raw data	38
A.4 Description of the CPs used as ancillary/auxiliary data	39
A.5 Internal QC by image provider.....	45
A.6 Additional EQC results representation	46
References	49

List of Figures xlix

List of Tables

Abstract

The main objective of the present study is to assess whether Pléiades-1A sensor can be qualified for Control with Remote Sensing (CwRS) programs, specifically in Common Agriculture Policy (CAP) Controls image acquisition campaign. The benchmarking presented herein aims at:

- evaluating the usability of Pléiades-1A for the CAP checks through an estimation of its geometric (positional) accuracy,
- measuring the influence of different factors (angle of view, number of GCPs, orthorectification model) on the above-mentioned accuracy.

For that purpose, the External Quality Control of Pléiades-1A orthoimagery conforms to the standard method developed by JRC and follows a procedure already adopted in the validation of previous VHR products.

Acknowledgments

The authors would like to thank F. Ranera (Astrium) and T. Westin (Spacemetric) for generating the orthoimagery considered for benchmarking and validation throughout this study. They also acknowledge their numerous comments regarding the outcomes of the benchmarking and their useful suggestions for the redaction of this document.

1 Introduction

The geometric validation of Pléiades-1A ortho products for use in CAP checks is based on the External Quality Control of orthoimages as an assessment of their planimetric accuracy, and follows strict guidelines enounced by JRC.

1.1 Objectives

The EU standard for the orthoimagery to be used for the purpose of CAP checks requires appropriate quality of the input data, as well as the quality assessment of the final ortho products [1]. Namely, the **prime sensor requirement** derived from ASPRS 1:10.000 scale map accuracy standards implies that the planimetric accuracy – also referred to as horizontal accuracy – of the orthoimagery, expressed as the Root-Mean-Square Error (RMSE) in Easting and Northing directions, should not exceed $2.5m$ to fulfill the geometric requirements and specifications of VHR products used in the CAP checks [2]. In this context, the purpose of the current study is to **perform initial geometric quality tests** with respect to the capabilities of the newly launched Pléiades satellite (presented in Section 2). The orthorectified imagery is assessed from a geometric perspective through External Quality Control (EQC), also referred to as the absolute accuracy check (see Annex A.1).

For the purpose of the (first) assessment of the Pléiades-1A data for use in CAP checks [3], a **benchmarking** of few selected images from Pléiades-1A orthoimage datasets provides a (limited) quantitative feedback on the geometric accuracy of the sensor. The quality assessment and validation of a given image adopts the workflow of [4, 5] which consists in two main phases [6, 7]:

- [a.1] the rectification phase (see Section 5): initial geometric correction of the primary image, a sensor orientation, and a space resection or bundle adjustment; following, orthorectification and resampling, that is the terrain/relief related distortion elimination based on sensor and terrain information (Digital Surface Model, DSM, or Digital Elevation Model, DEM), and Ground Control Points (GCPs) fitting to a new grid of rows/columns,
- [a.2] the EQC phase (see Section 6): estimation in the final ortho-product of the RMSE between the true location and the position on the orthorectified image of Independent (ground) Check Points (CPs) – *i.e.* points not included in the orthorectification process and derived from an independent source,

where the accuracy specifications on the auxiliary data (GCPs, ICPs and DEM/DSM) given by JRC in the so-called "**Guidelines for Best Practice and Quality Checking of Ortho Imagery**" [8] should be strictly followed. In practice, the EQC aims at checking that $RMSE_{1D} \leq 2.5m$ over the benchmarked images, where $RMSE_{1D}$ denotes the RMSE in both Easting and Northing directions.

2. Pléiades sensor

1.2 Context

The present benchmarking was subject to several practical constraints:

- Due to a tight schedule¹, a quick feedback to the image provider (Astrium) and the contractors on the performance of the Pléiades satellite was necessary; in particular, the input images were acquired right after the launch of Pléiades-1A (see Table 1) during the winter season. In particular, at the time of the study, there was insufficient radiometric information in order to complete all tests envisaged. This was considered a possible risk with moderate to high impact on the final EQC results. Also, as the imagery were already acquired and fixed, there were no preventive measures that could be taken in order to mitigate the possible adverse effect. Therefore, the first priority was to perform the test on geometric accuracy, for which a sufficient amount of ancillary was available.
- For that same reason, an AOI located in the JRC test zone of Maussane (see Section 4.1), for which sufficient ancillary and reference data already exist, was chosen for benchmarking. However, no new field campaign to gather a new set of auxiliary data was operated.
- Another crucial pre-condition for validation was that the (RPC and/or Rigorous) software versions for orthorectification were available on the market (see Section 3), before the introduction of Pléiades in CAP checks campaigns.

In that context, the scope of the current test by no means can validate the use of Pléiades-1A for the Land Parcel Identification System (LPIS) QA, which has higher demands on GSD and radiometry. Indeed, the geometric assessment is to be seen as a first phase of a complete validation procedure that also includes the radiometric assessment and the area validation (measurements).

The rest of the report is organised as follows. Next Section introduces the Pléiades sensor and its main properties. Section 3 presents the adopted benchmarking methodology and the processing workflow. Section 4 describes the primary imagery assessed for validation, and all other input data used for that purpose. Section 5 details the various ortho products generated for benchmarking in relation with the available input data. The results of the External Quality Control are presented and discussed in Section 6 together with the methodology used for the evaluation of the accuracy of the orthoimagery. Final conclusions

¹ It was thought in the first place that Pléiades-1A may be introduced as a speculative backup already in the 2012 years CAP campaign, while 3 demo products were made available elsewhere.

and statements regarding Pléiades-1A geometric assessment are drawn in Section 7 together with potential improvements for future benchmarking.

2 Pléiades sensor

The Pléiades system is composed of two twin satellites, Pléiades-1A and Pléiades-1B, operated as a constellation: on the same orbit and phased 180° one from the other. Therefore, this orbit phasing will allow – when both satellites will be operational – the satellites to revisit any point on the globe daily. The main sensor properties are summarized in Table 1. The reader is also referred to documents/publications released prior to Pléiades' launch for further information [9, 10, 11, 12]. It is important to note in particular, that Pléiades sensors acquire PAN and MSP raw images with $0.7m$ and $2.8m$ spatial resolution (Ground Sampling Distance, GSD) *resp.* Some restoration techniques – which imply mainly deconvolution/denoising/compression algorithms and which include numerous parameters that have been assessed during the in flight commissioning period [13] – are then necessary to produce the commercialised PAN and MSP primary images with higher spatial resolution (*resp.* $0.5m$ and $2m$ GSD).

In terms of images collection, Pléiades sensors enable:

- the acquisition of large areas, mapping typically up to 5 contiguous strips of $150km$ each in a single pass, as well as multiple single shot (point) targets,
- multiple single acquisitions of $20 \times 20km$ during the same pass, typically 20 images within an area (territory) of $1000 \times 1000km$,
- a mix of both scenarios.

Pléiades sensors acquire in forward and backward (bi-directional) scan. Together with the fast slewing and the wide image swath of $20km$ at nadir, this leads to a rather high collection rate compared to other VHR sensors (*e.g.* QuickBird, WorldView-2, GeoEye-1). Besides, the satellite can scan in North-South, East-West or any other arbitrary direction (scan azimuth) in between.

Mission characteristics	
number of satellites	2: Pléiades-1A and Pléiades-1B.
launch	Pléiades-1A: December 16th, 2012 – Pléiades-1B: December 2nd, 2012.
mission lifetime	Minimal: 5 years; estimated: more than 10 years.
Orbital elements	
type	Sun-synchronous, 10:30am at descending node.
altitude	694km.

inclination	98.2°.
cycle	26 days.
revisit frequency	With $\pm 30^\circ$ incidence angle and one satellite, daily revisit above 40° latitude and 1-2 days revisit between equator and 40° ; with $\pm 40^\circ$ incidence angle and two satellites, daily revisit of any point on the globe.
Instruments properties	
optical system	The telescope is a Korsch type combination with 65cm aperture diameter, focal length of 12.905m, f/20, TMA optics.

3. Benchmarking methodology

spectral resolution	PAN: BW=[0.47 – 0.83] μm (black and white); MS bands: B=[0.43 – 0.55] μm (blue), G=[0.50 – 0.62] μm (green), R=[0.59–0.72] μm (red), NIR=[0.74–0.94] μm (near-infrared).
detectors	PAN array assembly: 5×6000 (30,000 cross-track) pixels; MS array assembly: 5 × 1500 (7500 in cross-track) pixels – each pixel having a size of 13 μm .
ground sampling distance	PAN: 0.7m; MS: 2.8m (at nadir).
spatial resolution	PAN: 0.5m; MS: 2.0m.
swath width	20km at nadir.
dynamic range per pixel	12 bits per pixel (at acquisition).
viewing angle	Standard: $\pm 30^\circ$; maximum: $\pm 47^\circ$.
pointing agility	Roll of 60° within 25s; pitch of 60° within 25s; 200km in 11s including stabilization time.
acquisition capability	450 images/day (up to 600).
instrument TM link rate	Rate of 465 Mbits/s in 3 × 155 Mbits/s per channel.
onboard storage	600 Gbits (Solid State Mass Memory).

Table 1: Main characteristics of Pléiades system. Orbital elements and instruments properties².

In the present benchmarking, only Pléiades-1A have been considered for testing, as only those data were available at the time of the study (see Table 1: dates of launch). Therefore, the use of the term Pléiades, with no mention of the sensor version, in the rest of this document, will always refer to Pléiades-1A imagery, if not mentioned otherwise.

3 Benchmarking methodology

The processing workflow adopted herein for benchmarking follows that of previous HR/VHR orthoimagery validation [4] and conforms to the standard methods developed by JRC [8].

3.1 Test cases definition

The planimetric accuracy $RMSE_{1D}$ of the orthoimages is affected by various influencing factors:

- in acquiring the primary products:
 - [b.1] satellite viewing angle(s) of the input scene/image data being rectified,
- in preparing the ortho products (phase [a.1] on page 4):
 - [b.2] quality of ancillary reference data:
 - [b.2.i] number, distribution and accuracy of Ground Control Points (GCPs), which in turn is controlled by the quality of the GCP source,

primary data	DEM	ancillary data GCPs #	model	implementation
PAN 4°	DEM	4	RPC	ERDAS
				PCI
				Envi
			PixelFactory RPC	
		rigorous	Keystone	
			PixelFactory rig.	
		6
9		
0		
PAN 22°
PAN 30°

Table 2: **Benchmarking configurations.** For every test case, an orthoimage is produced. In total, around 70 products are produced for the current benchmarking.

- [b.2.ii] accuracy of height data (DEM) for image correction,
- [b.3] operator's capacity: the precision in identifying and locating GCPs on primary image data, since this phase also influences the overall accuracy of the GCPs themselves and the output product based on them,
- [b.4] models/tools used for orthorectification:

[b.4.i] mathematical model used for sensor correction: RPC or rigorous; possibly, the order of polynomial functions (RPC), [b.4.ii] the implementation of that model into software platform;

- in evaluating the ortho products (phase [a.2] on page 4):

[b.5] auxiliary reference data: number, distribution and accuracy of Independent Check Points (ICPs) used for validation²,

[b.6] operator's capacity to identify ICPs on ortho image data.

It is claimed that having a strict control on the reference data and a sufficient proven quality, the results of the orthorectification are mainly influenced by the accuracy of the input data and the reliability of the geometrical model, and not by external factors. Hence, in order to evaluate the geometric accuracy of Pléiades ortho-products, the scope of the testing comprises the following:

3. Benchmarking methodology

- 3 primary images of different viewing (off-nadir) angles: 4°, 22°, and 30° are analyzed, hence addressing the potential influence of factor [b.1]; while both bundle (panchromatic: PAN, and multispectral: MS) and pansharpened images (natural colour: PSH) are made available by the image provider (Astrium), only the PSH are tested.
- Taking into account the quality of the ancillary reference data [b.2]:
 - as the output planimetric accuracy is quite sensitive to the input GCPs used during the image correction phase and orthorectification (factor [b.2.i]), 3 different input configurations are considered: 4, 6 and 9 modeling GCPs well-defined (derived from DGPS measurements) and well-distributed spatially, plus a configuration without (0) any GCP;
 - a single highly accurate raster DEM is used to reduce the influence [b.2.ii] of the grid spatial resolution and the height precision.
- As not only the measurement of CPs (GCPs and ICPs as well), but also their selection and identification (coordinates extraction) on the images constitutes the key for successful EQC assessment (influencing factors [b.3] and [b.6]), this task is handled by JRC and its realisation is based on the practice, experience and assumptions of a photogrammetry specialist. Additionally, the number and location of the CPs is chosen in accordance with JRC guidelines [8]. Exactly the same set of CPs is used for the

² Hence, the method for validation chosen herein consists in partitioning known ground points in two sets, the first used in the orientation-orthorectification model (GCPs) and the second to validate the model itself (ICPs) adopting the Hold-Out Validation approach of [14, 5].

generation of the various orthorectified products on the different software platforms in order to ensure the consistency of the software performance test (see next item).

- The products under evaluation are the images orthorectified using the above mentioned inputs. The orthorectification is performed on five independent image processing platforms (factor [b.4.ii]):
 - commercial off-the-shelf softwares ERDAS[®], Envi[®], PCI[®] (implementations of RPC models) and Keystone[®] (rigorous model) ,
 - "in house" Astrium software: PixelFactory[®] (both RPC and rigorous models) ,

providing distinct implementations of RPC and rigorous models (hence addressing influencing factor [b.4.i]). The orthorectification process is performed by the image provider for all above-mentioned softwares, except Keystone (handled by the software provider Spacemetric itself).

- In order to enable the comparative robustness between the different processing contexts (depending on the selected input data and methodologies), well-defined ICPs, with precision at least as accurate as that of the GCPs used in orthorectification, are considered for the evaluation of image correction performance (influencing factor [b.5]).

As a consequence, around 70 products are produced for the benchmarking, each one corresponding to a different test case, and controlled through the EQC procedure (see Table 2).

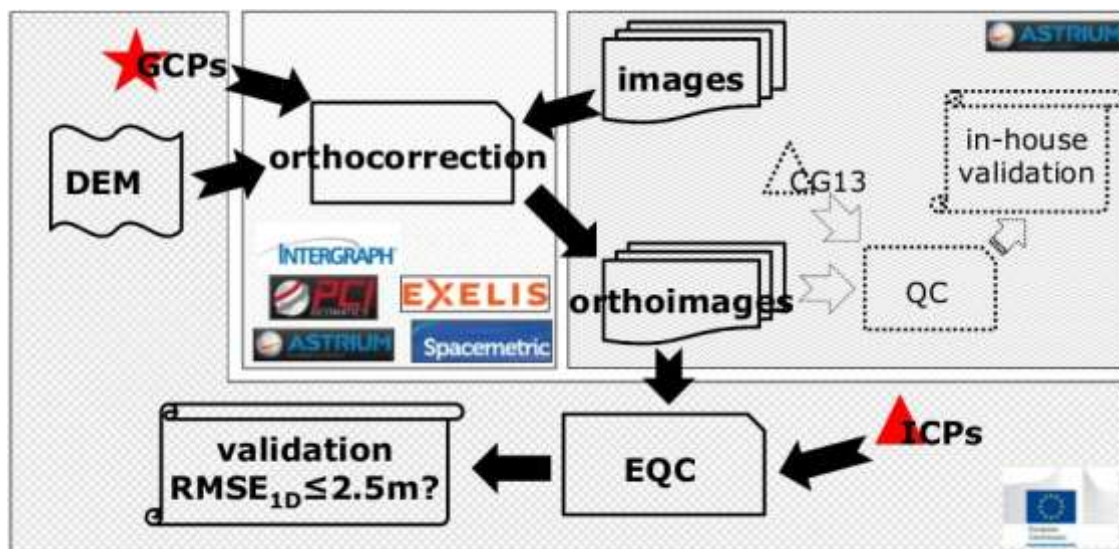


Figure 1: **Benchmarking workflow.** The different stages (i) to (iv) of the benchmarking are represented as dark bold items on the figure; stage (iv) is also represented as dashed items. See text for further description.

3.2 Test workflow design

The benchmarking workflow and the different assignments are represented in Figure 1. As mentioned earlier, it is systematic and conforms to the instructions and guidance developed by JRC and given in the "Guidelines for Best Practice and Quality Checking of Ortho Imagery" [8].

To summary, the whole process encompasses the different test cases presented in the previous section – cases [b.1] to [b.6] – and is composed of 4 main stages:

- (i) input data selection by the image provider (Astrium),
- (ii) ancillary data collection and selection by JRC,
- (iii) orthorectification on the different platforms by Astrium and a software provider (Spacemetric),
- (iv) EQC and validation by JRC.

Note in parallel the realisation of: (iv')

in-house QC by Astrium,

however this latter stage (whose results are presented in Annex A.5) is not considered for official validation.

4 Input data

For the various test cases to be elaborated, it is required to use in input (i) a set of primary raw images acquired with different viewing angles over a well-known area, and (ii) a set of

4. Input data



Figure 2: **Maussane test site**. Left: $10 \times 10\text{km}$ square **AOI** localisation in Southern France. Right: UltraCam aerial acquisition over Maussane.

well-defined ancillary data covering that same area: Digital Elevation Model and Ground Control Points. The input data used in the benchmarking are presented in this section.

4.1 Maussane test site and primary images

The test site of Maussane, located in France, has been selected for benchmarking by JRC (see Figure 2, left):

- a square 100km^2 subscene of images acquired over Maussane is defined for testing³: the AOI covers an extent of $10 \times 10 \text{ km}$ with UL corner at position (636223 E, 4846847 N) in EPSG 32631 (UTM - zone 31 N - ellipsoid WGS84) reference system⁴.

That same site has been used in previous HR and VHR validations [15, 4] as for the following reasons (see Figure 2, right):

- it presents a variety of agricultural condition typical for the EU, as well as urban settlements and water bodies,

³ A full scene testing should be scheduled at later stage.

⁴ The UL corner's location in Geographic Lat/Lon coordinates is: DMS=(43.76215 E,4.692342 N), or equivalently DEG=(43° 45'43.74⁰⁰ E,4° 41'32.43⁰⁰ N); see for instance the service: <http://itouchmap.com/latlong.html>.

- it contains a low mountain massif (650m above sea level) mainly covered by forest, surrounded by agricultural areas.

In addition, it offers:

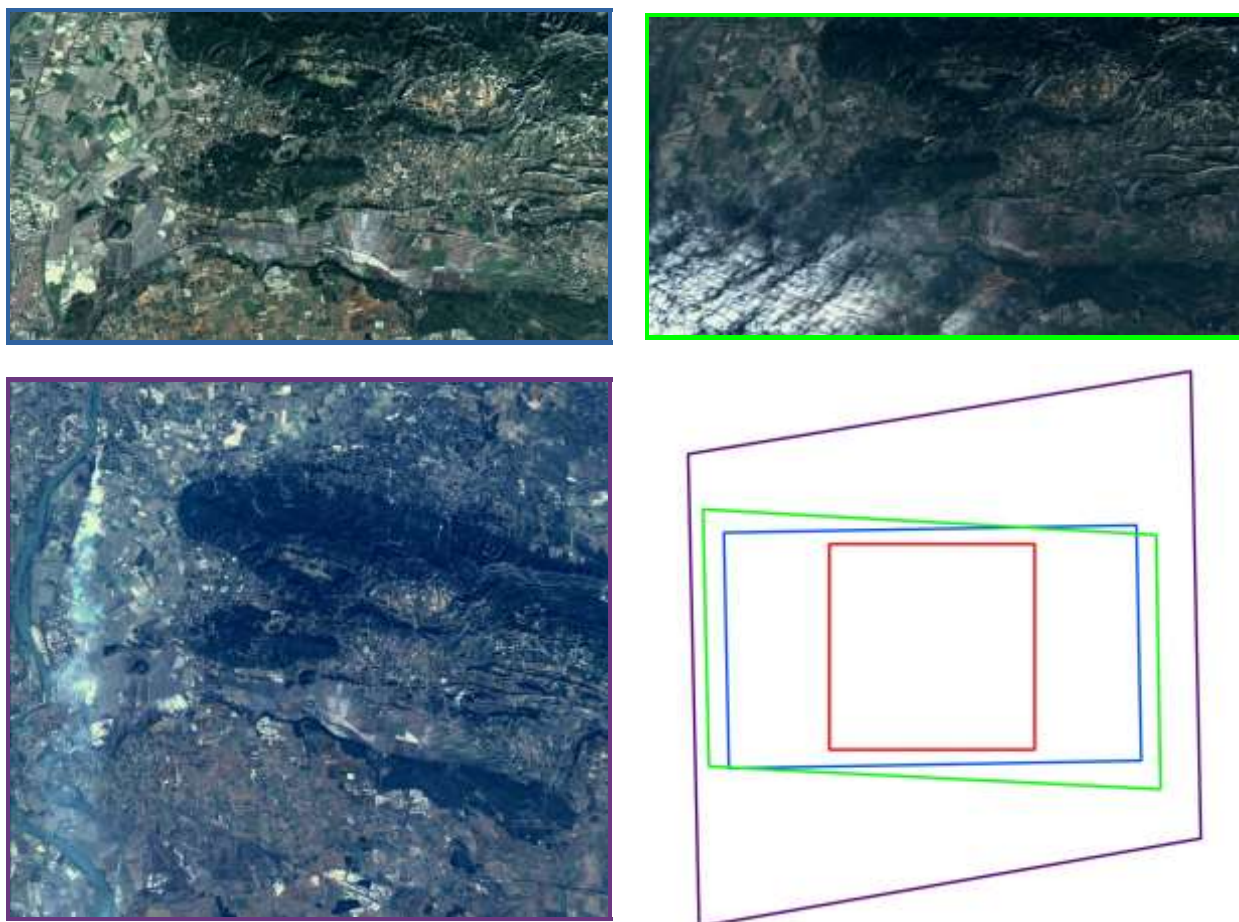


Figure 3: Pan-sharpened (natural colour) Pléiades acquisitions over Maussane and corresponding footprints. From top to bottom, from left to right: 4°, 22° and 30° primary products, and their corresponding footprints in EPSG 32631 reference system: blue, green and purple frameboxes resp. On this last figure, the Maussane AOI selected for geometric benchmarking is also represented as a red framebox.

- sufficient ancillary and reference data (GCPs, DEM) with a validated quality [16] (see next section),
- the possibility to test different viewing angles (considering Pléiades oblique viewing capabilities up to 47°; default is 30°).

As for the year 2012, 3 datasets (bundle: PAN and MS; PSH) over Maussane AOI have been acquired by Pléiades for geometric benchmarking (Figure 3):

- on 24/01/12 with angle around 4° ,
- on 12/01/12 with angle around 22° ,
- on 07/02/12 with angle around 30° .

4. Input data

Hence, as underlined in Section 1.2, the input images were all acquired during the winter season, with little to insufficient radiometric information.

4.2 Ancillary data: DEM and CPs

As for the selection of the Digital Elevation Model (DEM, required so that the elevation and curvatures of the earth can be taken into account in the orthorectification), it is specified in JRC guidelines [8, Section 8.3, Table 5]:

"DEM grid spacing [should be] 5 to 20 times that of the orthoproduct pixel size, depending on the terrain flatness, and DEM height accuracy [should be] $2 \times$ planimetric required $RSME_{1D}$."

In the context of VHR validation, it is usually accepted that the accuracy of DEM should be better than $5m$ when the incidence angle is lower than 30° , and better than $2m$ for incidence angle higher than 30° . Hence, a high-resolution/high-precision raster DEM with ellipsoidal heights is used for benchmarking:

- spatial grid of $2 \times 2m$,
- vertical accuracy $RMSE_z \leq 0.6m$.

The original DEM was produced from digital airborne stereo image pairs (Leica Geosystems) of GSD of $50cm$ in the frame of ADS40 project [16]. From that DEM, a subset is extracted so that a $500m$ -wider scope area than Maussane AOI is enclosed in the DEM AOI (see Figure 5).

Control Points (simply denoted CPs) retrieved from already existing datasets of GPS measurements over Maussane test site serve for the orthorectification of the images and the geometric quality validation of the derived orthoimages. Namely, 3 CPs datasets are considered [17, 16]: ADS40 and Vexel projects, and multipurpose use campaign, for defining the GCPs used in both the orthorectification and the validation (then called ICPs instead), provided the fulfilment of the accuracy requirement of JRC guidelines [8, Section 7.1]:

"GCPs [and ICPs] should be at least 3 times (5 times recommended) more precise than the target specification for the ortho, e.g. in the case of a target

RSME_{1D} ≤ 2.5m, the GCPs [and ICPs] should have a specification of RSME_{1D} ≤ 0.8m.”

Those conditions are indeed met considering the properties of the CPs for all considered datasets⁵:

- positional accuracy RSME_{1D} of at least 0.5m,
- vertical accuracy RMSE_z of at least 1m.



Figure 4: Example of ground camera shots of GCPs positioning. The ground accuracy of some of the GCPs used for orthorectification (GCPs #1 and #7 are displayed here) can be challenged.

4.3 Known issues on ancillary data

- As mentioned above, the GCPs are retrieved from existing CPs datasets, instead of being *selected in the images prior to be measured in the field* as JRC best practice suggests [8, Section 7.2]. Therefore, those points are subject to some limitations owing to the properties of the previous VHR validation campaigns they were selected for. The identification error of GCPs on the primary Pléiades image – hence, on images different from the original reference images, *e.g.* UltraCam image for the ADS40 campaign – may change the positional accuracy estimation as those points are more difficult to locate on the images (see Figure 4). Note that a similar remark applies to the ICPs selected for validation (see Section 6.1). In order to remedy the lack of accurate CPs for controlling VHR satellite imagery, it is suggested to operate in the future a new field campaign on Maussane test site to perform new ground measurements and gather a suitable set of reference points.
- The DEM used herein is in fact a DSM (Digital Surface Model), and, as so, it may create noise and have significant effects on the ortho image accuracy (*e.g.* in cases of high off-nadir viewing angles). The ortho product should be improved by applying an

⁵ Ideally, it should also be re-evaluated whenever a more accurate reference data is available.

intermediate processing step as a DSM → DTM filtering of the DEM provided by JRC⁶. However, in order to make results comparable between the different softwares, all actors were requested to apply the same process with the same reference data (GCPs and DEM), hence the DEM is used as it is (unfiltered) throughout the experiments.

- Note that the importance of the input ancillary data was already pointed out in previous QA studies on WorldView-2 imagery [5] as:

“With regards to ortho-image validation, the goal stated by the European Commission Services [...] can be reached provided that good quality Ground Control Points and DSMs are used.”

⁶ A DSM represents the Earth’s surface and includes all objects on it, for examples, buildings and trees. Many applications require the DTM which represents the bare ground surface without any objects.

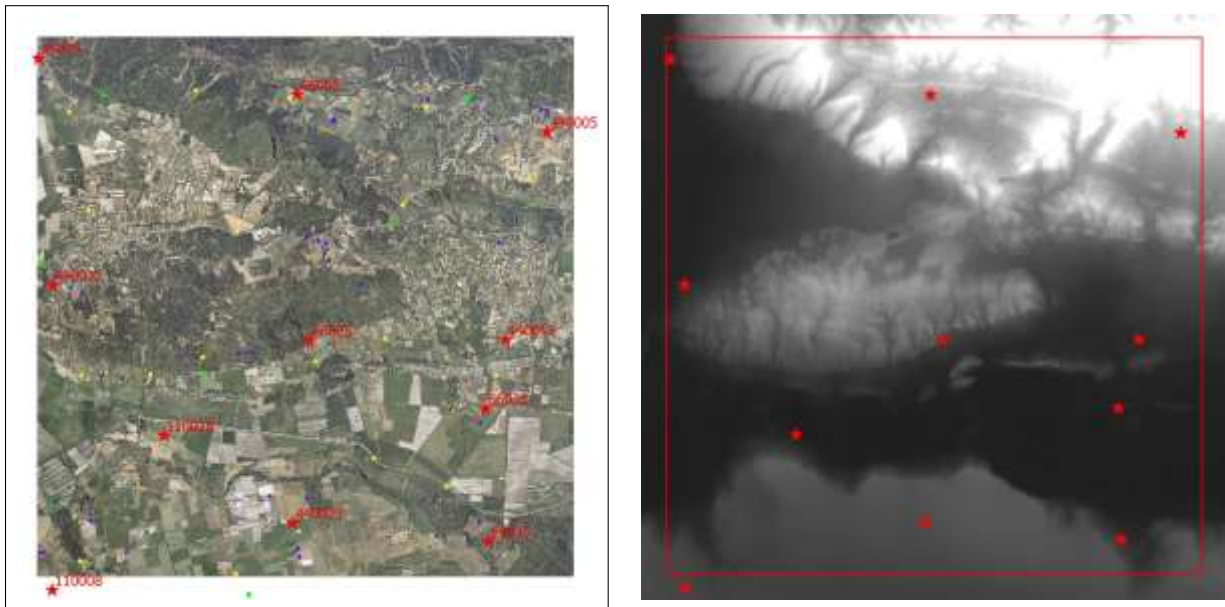


Figure 5: Overall selection of the GCPs over Maussane site and use in ortho products generation. Left: UltraCam aerial acquisition (same as Figure 2, right) and distribution of GCPs (red star F) over Maussane AOI; measurements of ADS40 project (green disk symbols ●), Vexel project (yellow diamond symbols) and multipurpose campaign (purple triangular symbols ▲) are also represented. Right: GCPs represented over the (georeferenced) DEM covering Maussane AOI (all 11 GCPs together); on this latter image, the AOI of Maussane is displayed as a red frame. Note that one of the GCPs (#110008) lies outside the AOI.

In particular, it is specified regarding the use of an appropriate DSM [5, Section "Future possibilities"] that:

"The mean accuracy of the used DSM should always be assessed by considering available Ground Points, and possible bias should be removed. [...] In order to obtain results that satisfy European Commission Services guidelines using WorldView-2 imagery, appropriate DSMs accuracy should be assessed."

5 Orthorectification process

The orthorectification of primary images combines relief effects corrections, georeferencing, and high location accuracy. This section outlines this process and its preparation – using different input data and methodologies – for benchmarking from the perspective of checking the final product geometric quality.

5.1 Ancillary modeling data preparation

Related to the (*in-situ*) selection of GCPs suitable for orthorectification, a general criterion is enounced in JRC guidelines as [8, Section 7.2]:

		GCPs					
#	ID	4	6	9			
1	66003						√
2	440011	√	√	√	√	√	√
3a	110008	√	√	√	√	√	√
3b	110016		√	√	√	√	√
4	66005						√
5	66025				√	√	√
6	440023	√	√	√	√	√	√
7	440005						√
8a	440015						√
8b	66031	√	√	√	√	√	√
9	66035						

√√√

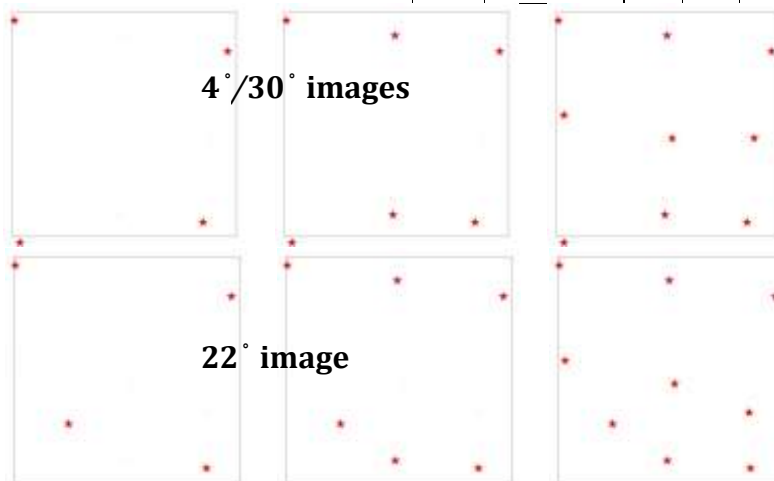


Figure 6: **GCPs configurations.** Left: GCPs selection for the creation of the ortho-products. Right: GCPs (red star **F**) spatial configuration for the 4° and 30° images (top), and the 22° image (bottom); from left to right: 4, 6 and 9 GCPs selected.

“it is important that the selected points are well-defined on the images and that they could be measured accurately”.

Instead, considering that the CPs (GCPs, but ICPs as well; see Section 6) used in the current study are retrieved from existing datasets – hence, no field campaign was performed (see Section 4.3) – the relevant criterion retained here is that:

“the selected points are well-defined on the independent source (e.g. map) should the point not be surveyed directly.”

Namely, the selection of GCPs consists in two steps:

- the localisation in an independent reference image: a preliminary set of GCPs is defined over Maussane AOI based on radiometric and/or spatial outstanding features extracted in a georeferenced VHR aerial image (UltraCam aerial acquisition: see Figure 5, left),
- the identification in the primary products: the GCPs that are easy to identify in the images are kept (see Figure 7); finally, those (at most 9 for each primary product) whose spatial distribution coarsely respects the 3×3 spatial pattern of von Gruber points (like a 6 on a dice) are selected [7].

In addition, the selection of GCPs is made taking into account the spatial distribution of points as GCPs should be well distributed over the AOI [8]. For consistency, this operation is performed by a single human operator, who performs also the EQC of the various ortho products⁷. Accordingly, 11 GCPs in total are selected over the PSH images (see Figure 6):

- 7 CPs commonly by all products,
- 2 CPs for both 4° and 30° images, but not the 22° image (owing, in particular, to the fact that this latter image displays an important cloudy area in the South-East region of the AOI that makes the localisation of CPs difficult),
- 2 CPs for the 22° image only,

and used in well-defined spatial configurations for benchmarking. Those are coarsely represented over the primary images in Figure 7. See also the Annex A.4 for further description of the used GCPs (and ICPs): available metadata information regarding the selected points in Table 8.

⁷ Similarly, ICPs chosen for error measurement should be precise and easy to identify; see Section 6.



Figure 7: **Localisation over the primary images of the GCPs used for orthorectification.** From left to right: GCPs selected over Maussane test site for the 4°, 22° and 30° images resp. (red star F, at most 9 for each image). See also Figure 6.

5.2 Ortho data production

Orthorectification methods can be classified in two categories: physically based models, which take into account several aspects influencing the acquisition procedure, and purely empirical ('black-box') models, independent of sensor characteristics or specific platform and acquisition geometry [18, 19, 6, 8, 14]:

- A rigorous sensor model describes the entire acquisition process in its fundamental physical/geometric aspects, including sensor/platform-specific information *e.g.* (provided as metadata: satellite orbital parameters, the attitude angles and the interior orientation parameters, ...), atmosphere refraction effect, terrain morphology (using a DEM) and a possible final cartographic transformation. This way, it enables to reconstruct the physical imaging setting and transformations between the 3D object space and the image space. The initial parameters of the model are usually refined by estimating corrections values using a suitable number of GCPs.
- The most used black-box model is the Rational Function Model, according to which the object point coordinates are related to image pixel coordinates through rational functions (*i.e.* ratios of polynomials). The major drawbacks of this approach are the request for a large number of GCPs (to guarantee a sufficient redundancy), its high sensitivity to GCPs distribution, its lack of reliability in the presence of outliers and the possibility of heavy distortions in areas distant from GCPs. On the basis of this model, the Rational Polynomial Coefficients(RPC) – also called Rapid Positioning Capability – can be supplied by the image provider (*e.g.* distributed in the metadata) to offer an

efficient, accurate alternative to rigorous orthorectification⁸. The model can then be refined adding relatively few GCPs.

There is always a trade-off between models accuracy and stability; using few parameters in the models will give stable results with few GCPs, using larger numbers of parameters will give possibility for a more accurate model but will then require larger numbers of GCPs to give reliable results.

In practice, the ortho-correction of Pleiades PSH data was operated by⁹:

- the image provider Astrium whenever ERDAS, Envi, PixelFactory and PCI softwares were used to generate the ortho-products,
- the software developer Spacemetric when employing Keystone.

As stated earlier (see Section 3), all GCPs (and ICPs) are identically chosen for each software-respective test in order to ensure the consistency of the software performance test.

5.3 Known issues on the orthorectification process

- Following the remark of Section 4.3 regarding the nature of the input DEM used in this study (which is in fact a DSM), deformations – like those noticeable in Figure 8, top – are observed in the ortho products. The output product can be improved using a DSM → DTM filter (see Figure 8, bottom). Note that similar artifacts were already observed with WorldView-2 images orthorectified using the same input DEM [4].
- Experiments in the field of human/machine computer vision [21] show that (i) the human eye is biased¹⁰, (ii) the precision of a mathematically based model cannot be reached in feature detection, neither can its systematicity. Hence, the subpixel precision reached – in locating CPs – by human measurements is questionable compared to accurate computer/mathematical models. Note moreover that it is also rather arbitrary, as it is essentially explained by the display precision of the software used for the localisation of the CPs. As noted before, the accuracy of the reference CPs cannot be simply reduced to the accuracy of the device used for GPS measurements, it should obviously take into account the accuracy in locating them; this error should ideally be measured and incorporated in the final assessment.

⁸ Note that the RPC are calculated in the "rigorous" way by a "blind" rigorous model owned by the image provider [20].

⁹ Precisely, the software versions used for the various processing were: PCI: 2013, ERDAS: 2011 – release 2011.0.5, Envi: 5 – Service Pack 1 (version classic), PixelFactory: 4.0 – Patch 6 and Keystone: 3.1.

¹⁰ The eye's response may be a performance limiter. In addition, note that to reach a consensus in human measurements, a collection of individuals is in general required; this approach is to be opposed to traditional photogrammetry processing, where measurements are performed by a single operator [21, 6].

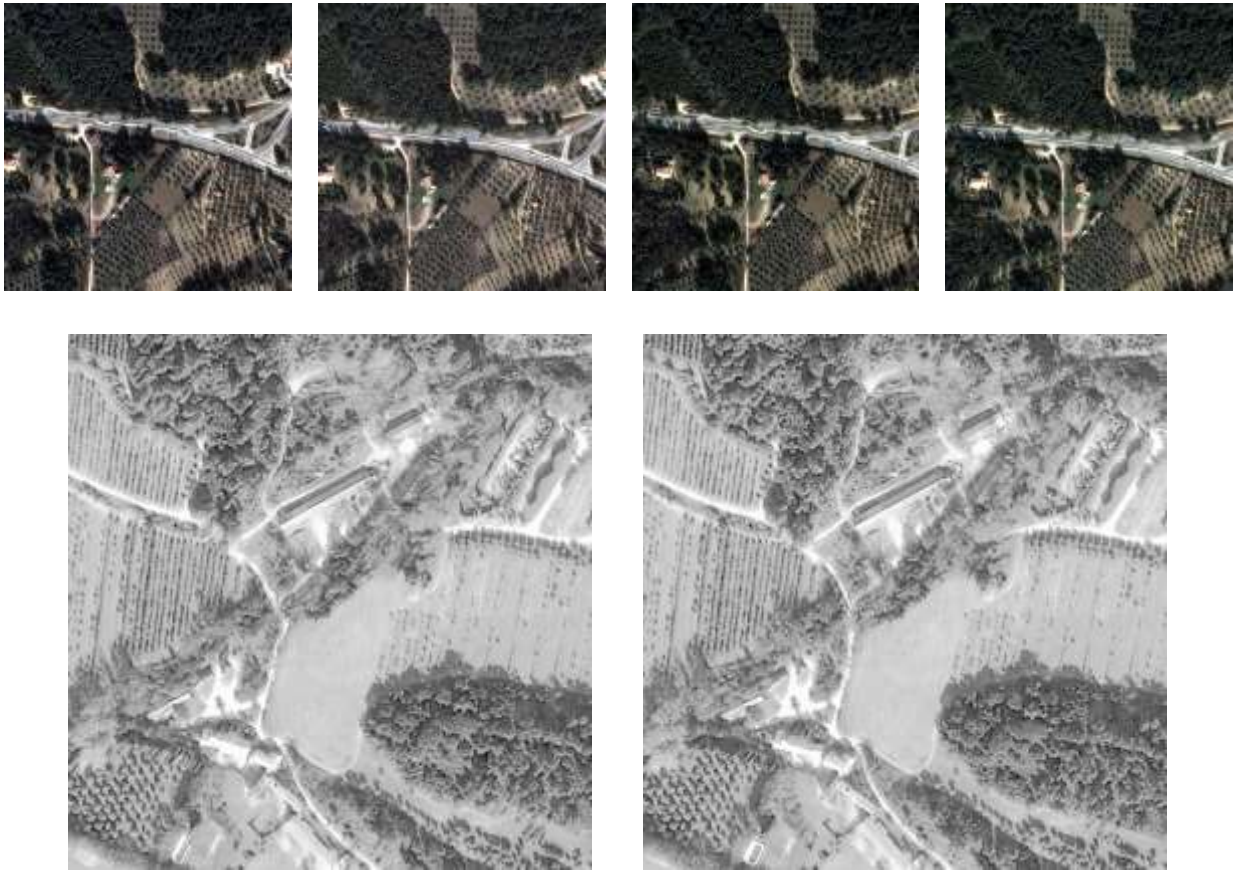


Figure 8: Artifact due to the use of a DSM instead of a DTM in the orthorectification.

Top: artifacts observed in some output orthoproducts derived from the 30° image; from left to right: ERDAS products with 0 and 9 GCPs, PixelFactory products with 0 and 9 GCPs; deformations ('warping-like' effects) are observed along the road and in the forest areas. Bottom (courtesy of Astrium): artifact reduction by the use of an actual DTM in the orthorectification; a PAN excerpt produced using the input DEM displaying artifacts (left) is compared to the same excerpt produced after a prior DSM → DTM filtering of the input DEM (right).

- Even if one person and one only performs the above-mentioned operations, the systematicity of the provided measurements can be questioned¹¹. It is believed that the QC of the ortho products (in both preparation and evaluation) should be automated – like other quantitative analysis of EO data [6]. By automatizing the process (e.g. through localisation from image chips correlation), errors could be reduced to one single possible source: the initial localisation of the GCPs (similarly, that of ICPs) in the reference image by a human operator, that will enable the production of reference image chips. It also eventually provides well-defined criteria (e.g. through the

¹¹ People have a limited attention span, which makes them susceptible to distractions; people are also inconsistent. Individuals themselves often exhibit different sensitivities during the course of a day or from day to day. Similarly, there are inconsistencies from person to person, from shift to shift, and so on [22].

optimisation of a correlation function) for localising CPs, and finally enables accuracy measurements (where numerical precision is reached).

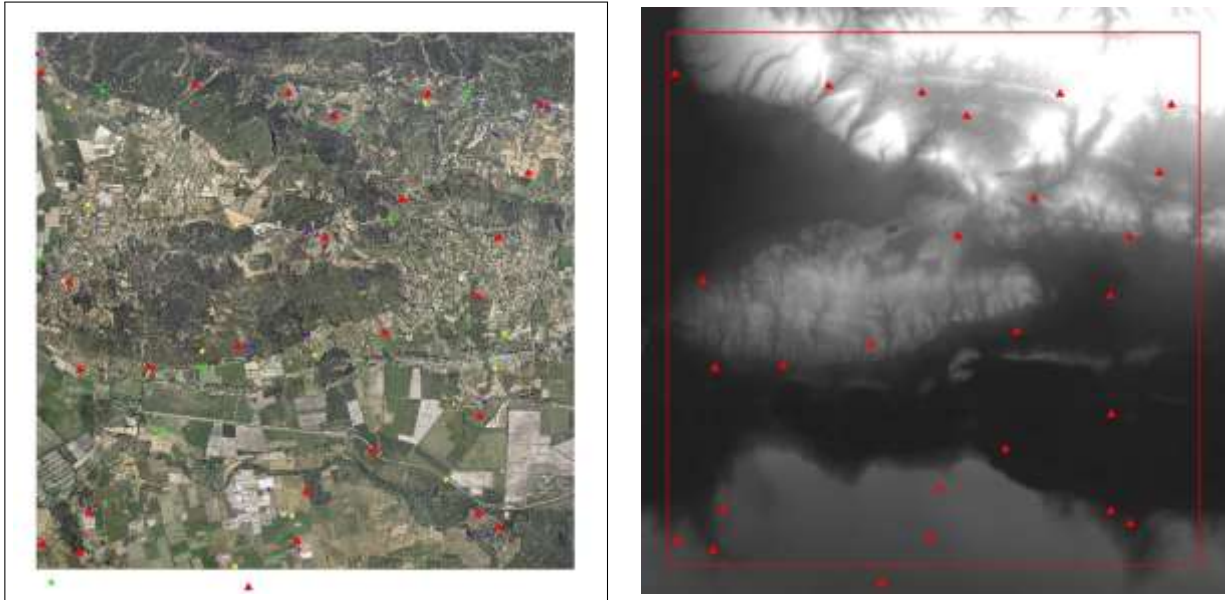


Figure 9: Overall selection of the ICPs used in EQC assessment. Left: ICPs are displayed over the UltraCam acquisition of Maussance (same as Figure 5, left) as red triangular symbols \mathbf{N} .

Right: ICPs displayed over the input DEM; the \mathbf{AOI} is also represented as a red frame over the image. See Figure 5 for additional features and comparison with the GCPs spatial distribution. Note that one of the ICPs lies outside the AOI.

6 External geometric quality control

The external quality control of the ortho-rectified product (geometric) accuracy is done by measuring the misregistration of Independent Check Points, using one parameter: the maximum permissible planimetric error $RMSE_{1D}$. The results output by this procedure and the final validation are presented in this section.

6.1 Auxiliary validating data preparation

In order to evaluate the geometric characteristics of the orthoimagery produced using different input data and methodologies, it is enough to perform the EQC, that is to check its (geometric) accuracy on a set of independent points (ICPs):

- that were not included in the orthorectification model definition,
- whose ground coordinates are (known and) derived from other (possibly more accurate) source,
- whose image coordinates are (identified and) used as reference.

Namely, the accuracy is evaluated as the $RMSE_{1D}$ of the residuals (see next section) between the orthoimagery derived coordinates of this set of points and their true ground coordinates¹².

¹² Equivalently, it can be evaluated as the residuals between the orthoimagery derived locations of this set of points and their identified (image) positions.

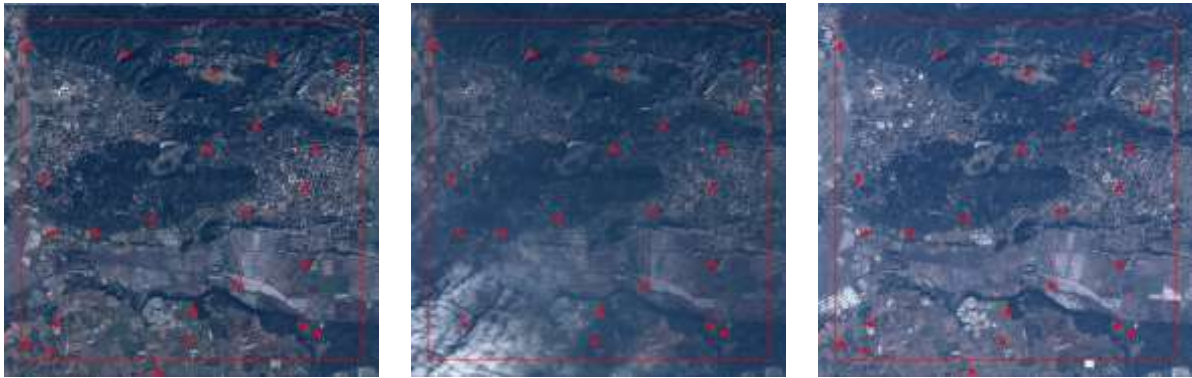


Figure 10: **Identification over the ortho-products of the ICPs used for validation.** From left to right: ICPs displayed (red triangular symbols \mathbf{N}) over the 4° , 22° and 30° orthoimages produced using PixelFactory software. See also Figure 7.

This approach is referred to as the Hold-Out-Validation method in [5].

In that context, a set of ICPs is selected that will remain unchanged for all tested ortho products. In order to provide both spatially and statistically significant results, these ICPs are:

- in sufficiently large number,
- and well-distributed on the entire image.

Hence, twenty six – *resp.* twenty two – ICPs are selected to evaluate the geometric accuracy of Pléiades 4° and 30° – *resp.* 22° – ortho images in horizontal direction (see Figure 10). Following, the identification of ICPs is repeated over each ortho product (see Figure 11). In practice, this operation is performed by the same operator as the one involved in the GCPs selection. See the Annex A.4 for further description.

6.2 Error measurement

The statistical analysis of the (point) error residuals at all ICPs yields the planimetric RootMean-Square Error (RMSE) as a natural indicator of the overall geometric accuracy. This indicator is simply defined as the square root of the arithmetic mean of the squares of the values that represent the residual between the true (reference) coordinates and the coordinates measured on the image (expressed in the same coordinate system). It is estimated in both Easting and Northing directions, *e.g.* using the following expression in Easting direction:

$$\text{RMSE}_{1D}[\text{East}], \text{PMSE}_{1D}[\text{East}] = \sqrt{\frac{1}{n} \sum_{i=1}^n (\hat{E}(i) - E(i))^2}$$

where n is the total number of ICPs used in validation (e.g. $n = 26$ for 4° and 30° , $n = 22$ for 22°), $E(i)$ is the known Easting reference coordinate of the i th ICP and $\hat{E}(i)$ is the corresponding Easting coordinate retrieved by visual examination of the ortho product.

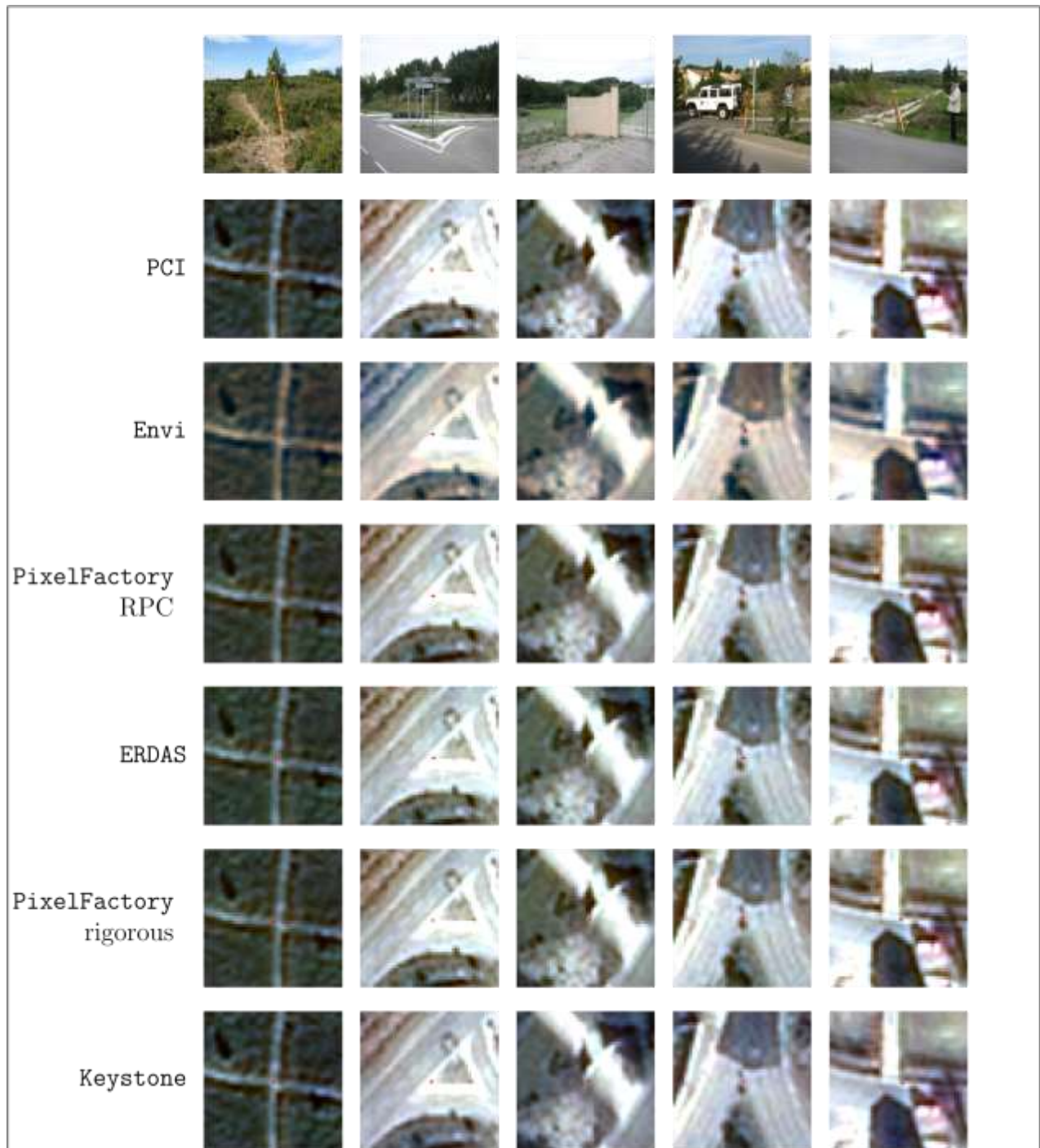


Figure 11: Localisation over the ortho-products of the ICPs used for validation. First row: ground camera shots of few selected ICPs. Second to last rows: the identification/localisation of ICPs shall be

repeated over the various ortho products; the excerpts show the (rectified) positions of these ICPs in the orthoimages as derived from their ground coordinates (red cross signs +).

Similarly in Northing direction, $RMSE_{1D}[North]$ is expressed as:

$$RMSE_{1D}[North], PMSE_{1D}[North] = \sqrt{\frac{1}{n} \sum_{i=1}^n (\hat{N}(i) - N(i))^2}$$

The overall accuracy of the transformation is evaluated by integrating residuals in both the Easting and Northing directions at all the ICPs used, namely the one-dimensional planimetric RMSE can be defined as:

$$RMSE_{1D}, \max\{RMSE_{1D}[East], RMSE_{1D}[North]\}.$$

Note that this indicator in fact includes two error components: the error of the source image (the one actually measured by the $RMSE_{1D}[East, North]$) and the (intrinsic) error of the point identification on the image (by the operator: see also Section 5.3 and related footnotes). Indeed, the value of the error of ICP identification on image varies from image to image, because it is influenced by the visual image quality. For example blur, shade, small contrast affects the process of point identification on target image. Also different acquisition date and/or plant phenologic phase may result in point identification error change.

Another accuracy indicator $RMSE_{2D}$ can be defined using the following formula:

$$RMSE_{2D}, PMSE_{1D}[East] + MSE_{1D}[North] = \sqrt{\frac{1}{n} \sum_{i=1}^n [(\hat{E}(i) - E(i))^2 + (\hat{N}(i) - N(i))^2]}$$

Although generally not considered for overall validation, it is also presented in the following evaluations.

6.3 Overall results

The overall results of the evaluation of the orthoimagery products selected for benchmarking (encompassing the test cases of Section 3.1, see Table 2) are presented in the Tables 3 and 4 (as numerical entries in the table), and displayed in Figure 12 (as markers in the graph). A quick overlook of these results shows already that:

- **$RMSE_{1D} \leq 2.5m$ is achieved as soon as $\#\{GCPs\} > 0$**

where, in fact, we have tested $\#\{GCPs\} \geq 4$ only. The $RMSE_{1D}$ over all ICPs is usually measured with values in Easting direction in the range $[0.35m, 0.85m]$, and with values generally higher in Northing direction in the range $[0.5m, 1m]$. In addition, the Figure 13 represents (altogether) the sensitivity of the orthocorrection *w.r.t.*:

- the number (and distribution) of GCPs used for a given orientation,
- the image viewing (off-nadir) angles,
- the mathematical model used for sensor orthorectification,

	GCP s #	4°		22°		30°		Envi 6
		East	North	East	North	East	North	
		[m]	[m]	[m]	[m]	[m]	[m]	
RPC models	0	6.2699	9.1535	9.4807	20.6989	4.0043	12.3516	
	4	0.8073	0.5249	0.9912	1.1581	0.6227	0.7599	PCI
	6	0.7435	0.4216	0.9942	1.1061	0.5655	0.8138	
	9	0.7511	0.4409	0.9229	0.9488	0.5460	0.8441	
	0	6.2405	9.1543	N/A	N/A	3.9949	12.2186	
ERDAS	4	0.5462	0.6349	0.3877	0.7933	0.6218	0.6418	
	6	0.5377	0.6673	0.4304	0.7775	0.5104	0.7370	
	9	0.5477	0.6739	0.5793	0.7666	0.6634	0.9422	
	0	6.2807	9.2093	9.7206	21.1338	4.0224	12.4055	
	4	0.7007	0.9166	0.6601	0.8624	0.9498	0.7395	
	9	0.5569	0.7876	0.4946	0.7009	0.8067	0.9930	
	0	5.7808	8.7620	9.2151	20.5021	3.3928	11.8586	
	4	0.5411	0.9451	0.4059	1.0443	0.5984	0.9059	
		0.6946	0.9049	0.5236	0.8203	0.8403	1.0297	
PF	6	0.5416	1.0033	0.3742	1.0668	0.6572	0.8853	

Rigorous models

0	3.5453	5.8054	9.8786	20.3306	3.8126	11.8778
4	0.4237	0.5250	0.3667	0.8499	0.6659	0.7250
Keystone						
6	0.3739	0.4844	0.4109	0.7480	0.5750	0.8183
9	0.3674	0.4312	0.4378	0.7220	0.4566	0.7076
0	5.8023	8.7351	9.2334	20.4757	3.4506	11.8133
4	0.4722	0.5655	0.3755	0.7462	0.5499	0.5311 PF
6	0.5941	0.3935	0.3832	0.7919	0.5347	0.7004
9	0.7051	0.5355	0.3982	0.7266	0.6743	0.6720

Table 3: Planimetric $RMSE_{1D}$ measurements per software suite. The $RMSEs$ in Easting and Northing directions are presented altogether for the different softwares (PF stands here for PixelFactory) and primary products considered for benchmarking. The East (resp. North) columns store the $RMSE_{1D}[East]$ (resp. $RMSE_{1D}[North]$) errors expressed in meters. Note that these entries are exactly those represented in the points cloud of Figure 12. For each image (hence, per column, disregarding the number of GCPs employed), the highest and lowest errors measured (models with 0 GCPs excluded) in both Easting and Northing directions using the available softwares are displayed as red and blue boxes resp.

			RPC				Rigorous	
off-nadir	GCPs	dir.	PCI	ERDAS	ENVI	PF	KS	PF
[angle]	#		[m]	[m]	[m]	[m]	[m]	[m]
4°	0	East	6.2699	6.2405	6.2807	5.7808	3.5453	5.8023
		North	9.1535	9.1543	9.2093	8.762	5.8054	8.7351
		2D	11.095	11.079	11.1471	10.4972	6.8024	10.4866
	4	East	0.8073	0.5462	0.7007	0.5411	0.4237	0.4722
		North	0.5249	0.6349	0.9166	0.9451	0.525	0.5655
		2D	0.963	0.8375	1.1537	1.089	0.6747	0.7367
	6	East	0.7435	0.5377	0.6946	0.5416	0.3739	0.7051
		North	0.4216	0.6673	0.9049	1.0033	0.4844	0.5355
		2D	0.8547	0.857	1.1407	1.1402	0.6119	0.8854
	9	East	0.7511	0.5477	0.5569	0.5465	0.3674	0.5941
		North	0.4409	0.6739	0.7876	0.9879	0.4312	0.3935
		2D	0.871	0.8683	0.9646	1.129	0.5665	0.7126
0	East	9.4807	N/A	9.7206	9.2151	9.8786	9.2334	
	North	20.6989	N/A	21.1338	20.5021	20.3306	20.4757	
	2D	22.7668	N/A	23.2621	22.4778	22.6036	22.4613	
22°	4					0.3667	0.3755	

30°	6	East	0.9912	0.3877	0.6601	0.4059	0.8499	0.7462	
		North	1.1581	0.7933	0.8624	1.0443	0.9256	0.8354	
		2D	1.5244	0.883	1.086	1.1205			
	6	East	0.9942	0.4304	0.5236	0.3742	0.4109	0.3832	
		North	1.1061	0.7775	0.8203	1.0668	0.748	0.7919	
		2D	1.4873	0.8887	0.9732	1.1306	0.8534	0.8797	
	9	East	0.9229	0.5793	0.4946	0.399	0.4378	0.3982	
		North	0.9488		0.7009		0.722	0.7266	
		2D	1.3236	0.	7666	1.0108	0.8444	0.8286	
	30°	0	East	4.0043	3.9949	4.0224	3.3928	3.8126	3.4506
			North	12.3516	12.2186	12.4055	11.8586	11.8778	11.8133
			2D	12.9845	12.855	13.0413	12.3344	12.4747	12.3069
		4	East	0.6227	0.6218	0.9498	0.5984	0.6659	0.5499
			North	0.7599	0.6418	0.7395	0.9059	0.725	0.5311
			2D	0.9825	0.8936	1.2037	1.0857	0.9844	0.7645
		6	East	0.5655	0.5104	0.8403	0.6572	0.575	0.5347
			North	0.8138	0.737	1.0297	0.8853	0.8183	0.7004
			2D	0.9909	0.8965	1.3291	1.1025	1.0001	0.8812
9		East	0.546	0.6634	0.8067	0.6443	0.4566	0.6743	
		North	0.8441	0.9422	0.993	0.8923	0.7076	0.672	
		2D	1.0053	1.1523	1.2794	1.1006	0.8422	0.952	

Table 4: Planimetric $RMSE_{1D}$ and $RMSE_{2D}$ measurements per orientation. The East (resp. North and 2D) rows store the $RMSE_{1D}[East]$ (resp. $RMSE_{1D}[North]$ and $RMSE_{2D}$) errors expressed in meters. For each selected method (depending on the number of GCPs used; hence, per row), the highest and lowest errors measured using the available softwares are displayed as red and blue boxes resp.

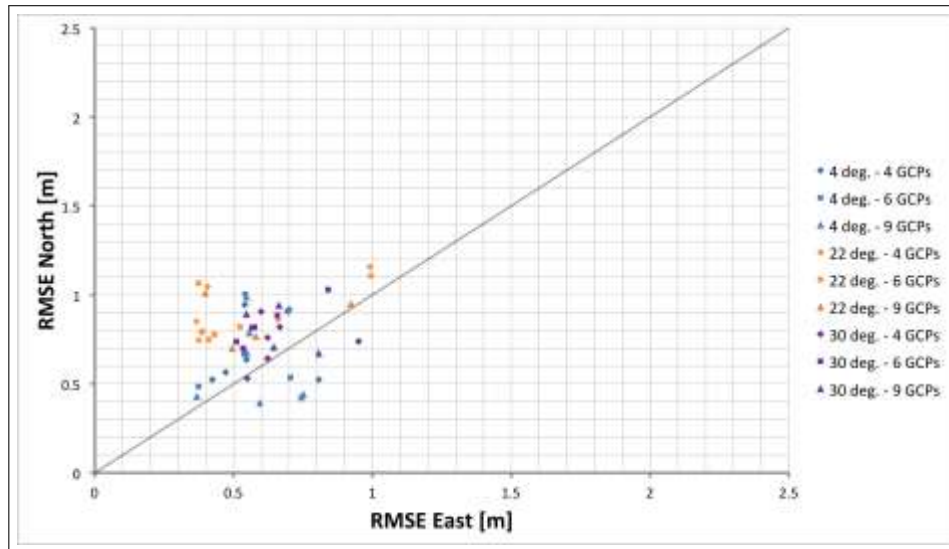


Figure 12: **Overall representation of RMSE_{1D} error.** Graph of RMSE measurements in Easting/Northing directions over ICPs selected by JRC where every single orthoimage, identified by the viewing angle of the primary input image (4°, 22° and 30°), and the number of GCPs used for orthorectification (4: , 6: or 9: N GCPs), is represented as an entry marker. CAP requirement RMSE_{1D} ≤ 2.5m (bounds of the graph) is fulfilled.

while evaluating their effect on ortho-image accuracy. When considering the RMSE_{1D} measured over all ICPs (see Table 5), the average accuracy is above the pixel size (*i.e.* 0.5m) in both Easting (RMSE_{1D}[East] ≈ 0.5828m) and Northing (RMSE_{1D}[North] ≈ 0.7745m) directions. Hence, the maximum average RMSE_{1D} error measured on ICPs is very well below the 2.5m CAP requirement in all orthoimagery products (again: as soon as $\#\{GCPs\} \geq 4$).

A closer analysis of Figure 13 and related Figures 14 (displaying RMSE_{1D} estimations for all softwares, all orientations and all configurations) and 15 (similarly displaying RMSE_{2D} estimations) further show that, in this specific study:

- the impact of the viewing angle on the RMSE_{1D} error is not clear as no obvious correlation is extracted (though, it is still < 2.5m when increasing),
- the increase of GCPs does not significantly improve the geolocation accuracy; owing

#	East North			angle	East North		
	East	North	2D		East	North	2D
4	0.5937	0.7705	0.9858	4°	0.5806	0.658	0.8920
6	0.5776	0.7951	0.9946	22°	0.5297	0.8689	1.0272
9	0.5770	0.7579	0.9637	30°	0.6379	0.7966	1.0248
					East North		2D

	overall	0.5828	0.7745	0.9813
--	---------	--------	--------	--------

Table 5: Average errors measured over ICPs in orthoimagery products. Top: both $RMSE_{1D}[East, North]$ and $RMSE_{2D}$ errors (expressed in meters) are averaged per number of GCPs used in the orthorectification (left) and per primary image orientation (off-nadir viewing angle, right). Bottom: those errors are averaged over all orthoproducts indistinctly.

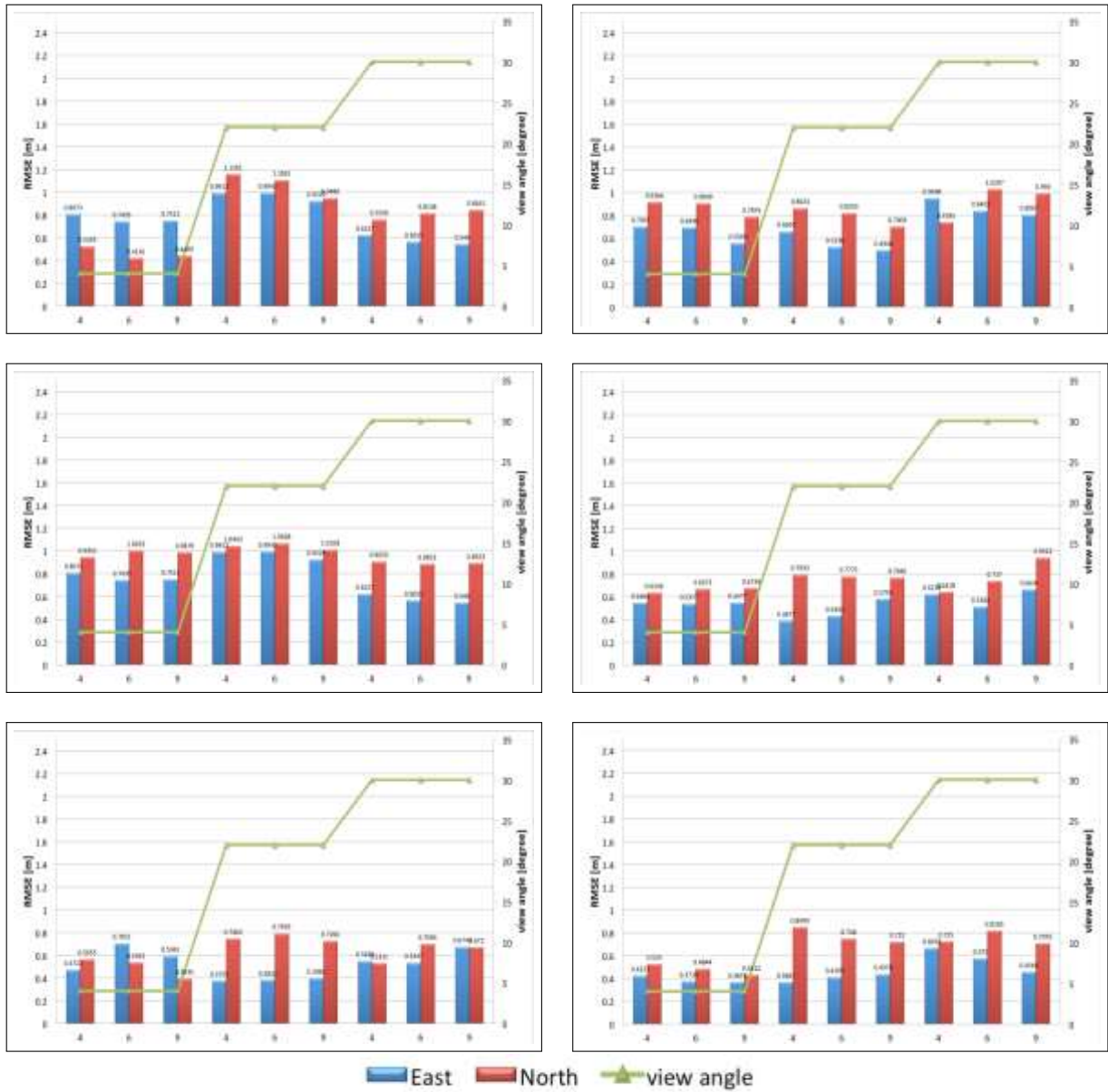


Figure 13: **Graph representation of error measured over ICPs.** The RMSE measured over the orthorectified products is represented as a function of the number of GCPs used in the orthorectification process for the different software suites and models (RPC and rigorous). From top to bottom, from left to right: the results using PCI, Envi, PixelFactory RPC, ERDAS, PixelFactory rigorous and Keystone resp. are presented. For each one of those softwares, both East and North errors (in blue and red resp.) for all 4°, 22° and 30° images (green steps) are displayed.

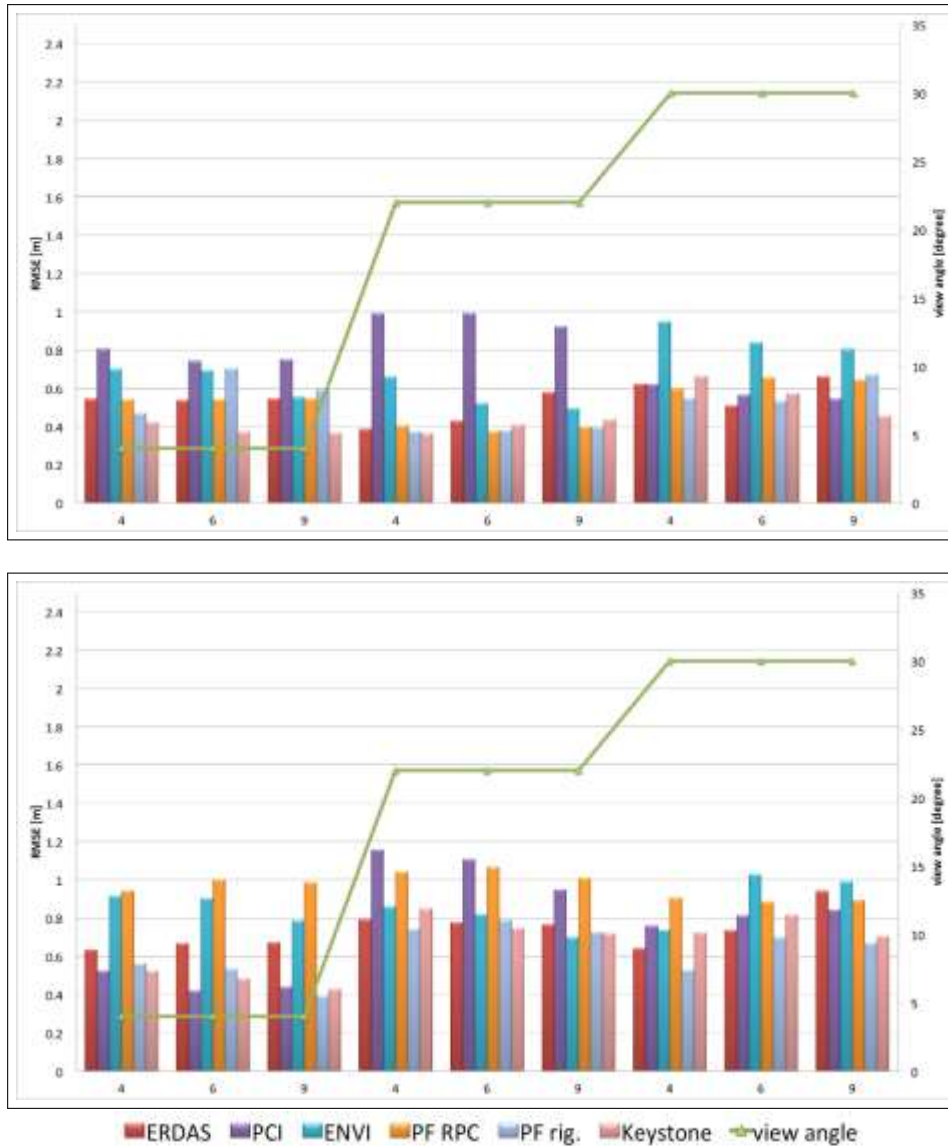


Figure 14: **RMSE_{1D} measurements: all software suites, all viewing angles and all GCPs configurations.** The planimetric RMSEs in Easting and Northing directions are represented altogether for the different softwares (PF stands for PixelFactory here) used in the orthorectification process: ERDAS, PixelFactory RPC, PCI, Envi, PixelFactory rigorous and Keystone, and the different viewing angles: 4°, 22° and 30°.

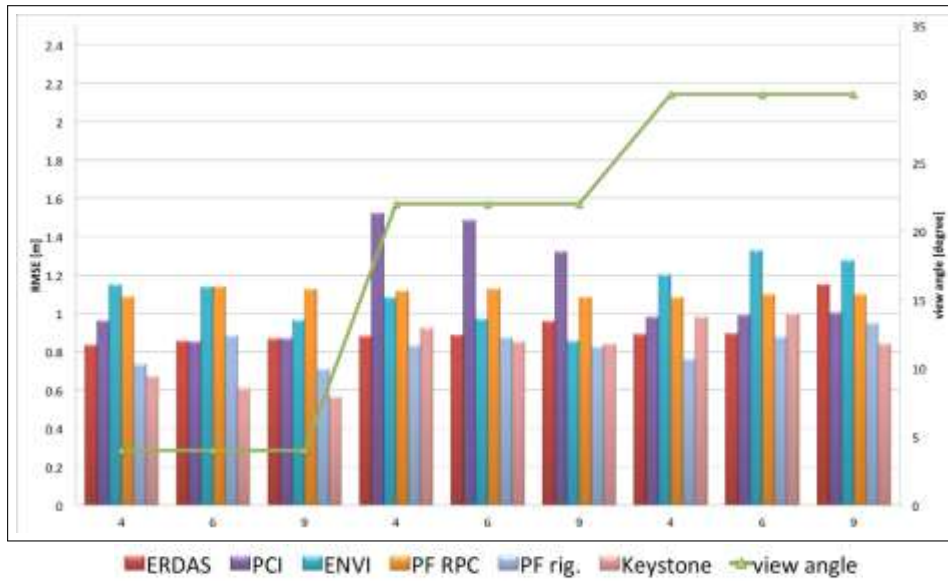


Figure 15: **RMSE_{2D} measurements: all software suites, all viewing angles and all GCPs configurations.** Similarly to Figure 14, the errors are represented altogether for the different softwares and viewing angles.

to the accuracy of the input ancillary data and the manual selection of the GCPs in the raw imagery (see Section 5.3), errors are most certainly introduced in the identification/localisation of the GCPs but neither evaluated nor quantified¹³,

- the use of rigorous models (with PixelFactory and Keystone softwares) globally provides better results than the use of RPC models (with Envi, ERDAS, PCI and PixelFactory); the fact that rigorous models provide better outputs could be explained by a lesser sensitivity to the quality of input GCPs (see previous item); in addition to a higher demand on GCPs, another drawback of RPC models is often their inability to model high frequency geometric variations (*e.g.* complex attitude variation).

The Figures 19 to 21 presented in Annex A.6 aim at further supporting those observations.

7 Conclusion

The main objective of the study presented in this document was to assess whether Pléiades sensors – specifically, Pléiades-1A – could be qualified for use in CAP checks (CwRS and LPIS). In practice, this means that the prime sensor requirement derived from the ASPRS 1:10.000 scale map accuracy standards, implying that the planimetric (horizontal) accuracy of the orthoimagery, expressed as the RMSE in both Easting and Northing directions, does not exceed 2.5m, should be fulfilled [2, 1]. For that purpose, a benchmarking was operated that

¹³ A similar comment applies for the identification/localisation of the ICPs in the orthoimagery.

aimed at both evaluating the geometric (positional) accuracy of Pléiades-1A orthoimagery, and measuring the influence of different factors (viewing angle, number of GCPs, orthorectification model) on the accuracy. The External Quality Control assessing the orthoimagery from a geometric perspective was performed in accordance with the standard methodology and guideline enounced by JRC [8]. With respect to the capabilities of Pléiades-1A, it is then herein verified that this sensor fulfills the geometric requirements and specifications of VHR products used in the CAP checks as:

- **the prime sensor requirement on planimetric accuracy $RMSE_{1D} \leq 2.5m$ is fulfilled** (as soon as $\#GCPs \geq 4$, and independently of the software).

Besides, as no evidence was disclosed, it is assumed that:

- the planimetric positional accuracy seems to be not correlated to either the viewing angle ($min = 4^\circ, max = 30^\circ$), or to the number of GCPs ($min = 4, max = 9$).

Hence Pléiades-1A is validated from the geometric perspective. Following, the overall radiometric quality and image content of the orthoimagery products [23, 24] should also be tested and validated (using for instance the data of Annex A.3). Area measurements should also further validate the data. Some criticisms addressed about the current EQC methodology – and already pointed out in [5] – regard the quality of the input ancillary and auxiliary, as those may introduce some bias and influence the orthocorrection process. In particular, dedicated and high quality ancillary data should be used:

- the accuracy of the DEM (which is a DSM and not a DTM) should be tested,
- GCPs (and ICPs) should be defined in-situ following a prior analysis of the raw primary images.

Though, note that this approach and the inherent comments feed the procedure for the qualification process of Pléiades-1B [3, 25].

Annexes A

A.1 Image quality control and assurance

The documentation regarding the “VHR image acquisition specifications for the CAP controls” [2, Section 13.1] provides conceptual definitions of appropriate Image Quality Control (QC) and Quality Assurance (QA):

- QA may be defined to be the steps performed in order to ensure that the production of a product meets a set of accepted standards. QC aims to detect non-conformities in a product.
- QC includes assessment of issues such as data integrity, completeness, cloud cover, haze or thin clouds, fog, smoke, smog, snow, flares and possibly cloud shadows, etc. It will proceed on the image product where geometry, radiometry, image characteristics

(dropouts, *etc*), production parameters (resampling algorithm, bit depth), *etc* are evaluated.

A.2 Orthoimage technical specifications for the purpose of LPIS

The technical specifications for the purpose of LPIS are reproduced in Table 6. A dynamic (regularly updated) version of this table is available at http://marswiki.jrc.ec.europa.eu/wikicap/index.php/Orthoimage_technical_specifications_for_the_purpose_of_LPIS, as well as further documentation.

DQ criteria	conformance level & tolerance limits	quality	notes	expected rate of conforming items
Geometric DQ criteria				
spatial resolution	$\leq 1m$		Ratio of the final ortho resolution to the GSD is 1:1 for digital sensors, whereas for film cameras should be at least 1.2 : 1.	100%
geometric accuracy	$RMSE_{ID} \leq 2.5m$		RMSE is calculated on the base of at least 20 well distributed independent check points (ICP), per image.	100%
Radiometric DQ criteria				
radiometric resolution	≥ 8 bits/channel		11–12 bits per channel is highly recommended.	100%
spectral resolution	color (natural or color infrared)		Panchromatic only (satellite or aerial) data is allowed, only if there is no option for color imagery.	100%
general image quality	lack of defects and artifacts, which could prevent the visual interpretation of the image		Checking for existence of scratches, dust, threads, hot spots, haze, drop lines, shadows, color seams, spilling, artifacts, <i>etc.</i>	N/A (no defects allowed)
cloud cover	$< 5 - 10\%$		Per image and in total, where the term "image" is used for the 'control unit', <i>e.g.</i> orthoimage, mosaic (map sheet).	100%

overall clipping	< 0.5% at each tail	The clipping metric is calculated on the luminosity histogram; the first 5 and last 5 bins of the histogram can be considered as belonging to the tail.	N/A
histogram peak	±15% of middle value	For 8 bit image, the middle value is 128.	N/A
color balance	< 2% between min and max value of triplet.	Difference between the minimum and maximum digital counts in the triplet calculated on nearly "neutral" objects (such as paved roads or building tops); this measure is not applicable for panchromatic only imagery.	N/A
noise	Signal to Noise Ratio (SNR) > 5 for each channel	SNR which is defined as the ratio of the mean DN value to the standard deviation of the DN values (calculated on areas of uniform density of middle values).	N/A
contrast	the coefficient of variation of the image DN values should be in the range of 10 – 20%	Represented as the Standard Deviation of the DN values as a percentage of the available grey levels.	N/A

Table 6: **Data quality (DQ) criteria of orthoimage.** Technical specifications for the purpose of LPIS.

The requirements for image geometric quality assurance followed in the present report are specified by the entries "spatial resolution" and "geometric accuracy" of the table.

For further information/clarification on image radiometric quality assurance, the reader is referred to the dynamic link http://marswiki.jrc.ec.europa.eu/wikicap/index.php/Image_radiometric_quality_assurance#Conclusion_and_follow-up (last visit on January 2013). Note in particular that, at the time of the publication of the present report, technical discussions were engaged between JRC and CwRS contractors regarding the quality measures related to radiometry and photometry given in the JRC guidelines and specification for orthoimagery [8]. As stated then, the quality expectations related to radiometry were considered as indicative and as recommended best practices, but there were no absolute conformity levels.

Table 7 provides with the list of HR/VHR spaceborne sensors that were accepted for CwRS (at the time of Pléiades' benchmarking), as reported in the webpage on orthoimagery accuracy http://marswiki.jrc.ec.europa.eu/wikicap/index.php/Accuracy_of_the_orthoimagery_used_in_CwRS (last visit on January 2013). The reader is also referred to

the webpage http://marswiki.jrc.ec.europa.eu/wikicap/index.php/VHR_spaceborne_sensors_suitable_for_LPIS_creation_and_update for further information on VHR sensors suitable for LPIS creation and update.

	data type	RMSE _{1D} [m]
	aerial photographs	2.5
	VHR PAN $\leq 1m$ satellite imagery (GeoEye1, Ikonos2, Quickbird, WorldView2)	2.5
	EROS A 1.8m satellite imagery single scene	2.5
	EROS A 1.8m satellite imagery vector scene (3.5
	THEOS Pan	4
	SPOT 5 Pan Supermode	5
	Formosat 2	5
	Rapid Eye Preprocessing 1B	5.5
	Rapid Eye Preprocessing 3A	8.5
	THEOS multispectral	15
	SPOT 5 multispectral	15
	SPOT 4 multispectral	30
	RADARSAT	20
	UK DMC II	25
	IRS P6 LISS III	40
	LANDSAT TM	50
	UK DMC	50

Table 7: Accuracy of the orthoimagery used in CwRS. List of existing validated sensors with their respective spatial resolution.

A.3 Additional primary raw data

Following the first acquisitions over Maussane test site (see Section 4.1), one extra prime imagery dataset (PAN, MS) was acquired during the summer temporal window for possible later radiometric benchmarking:



Figure 16: **Pan-sharpened Pléiades 16° acquisition over Maussane.** Left: additional 16° image acquired over Maussane test site, to be used for radiometric QA. Right: 4° image for comparison (same as that displayed in Figure 3).

- on 12/07/12 with angle around 16°.

The 16° data is displayed in Figure 16 (left), together with the 4° (right) for comparison. It was not used in the present study.

A.4 Description of the CPs used as ancillary/auxiliary data

The available information used to select (see Section 4.2):

- the GCPs provided for ortho-rectification,
- the ICPs employed in the EQC,

and locate them in – primary and ortho *resp.* – images (see Sections 5 and 6) is displayed in the Tables 8 and 10 *resp.*. The reader is referred to [17, 16] for further information regarding the considered CPs databases.

#	ID	source	screen shot	ground camera shot
1	66003	multipurpose		
2	440011	Vexel		
3a	110008	ADS40		
3b	110016	ADS40		

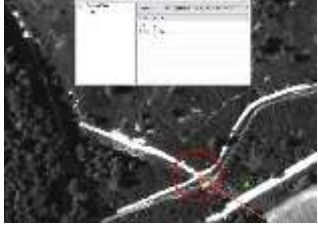
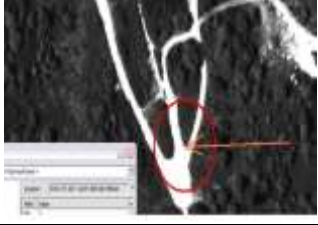
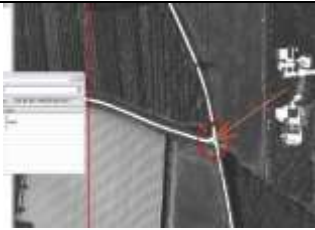
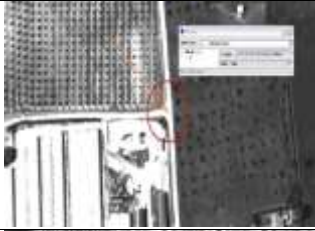
4	66005	multipurpose		
5	66025	multipurpose		
6	440023	Vexel		
7	440005	Vexel		
8a	440015	Vexel		
8b	66031	multipurpose		
9	66035	multipurpose		

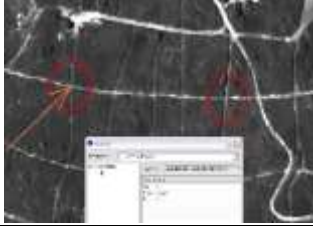
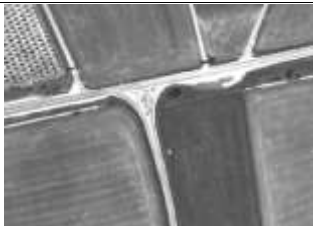
Table 8: GCPs selection over Mausanne site. GCPs from 3 different datasets (see Section 4.2) were selected and positioned on the primary imagery based on the available visual information (ground camera shots and image screenshots).

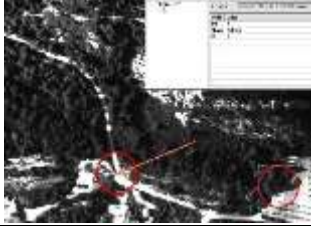
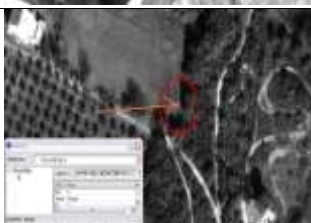
#	ID	ground position [m]		height [m]	
		North	East	ellipsoidal	orthometric
1	66003	4846448,28	636305,211	55,838	N/A
2	440011	4842244,515	636560,472	58,84	8,852
3a	110008	4836585,549	636561,549	80,238	30,296
3b	110016	4839449,608	638647,342	51,561	1,592
4	66005	4845775,194	641149,126	152,591	N/A
5	66025	4841215,071	641380,518	83,021	N/A
6	440023	4837826,921	641060,734	87,87	37,91
7	440005	4845076,105	645815,166	176,54	126,498
8a	440015	4841227,208	645030,5	60,33	10,326
8b	66031	4839947,753	644655,96	52,608	N/A
9	66035	4837489,03	644717,258	63,612	N/A

Table 9: Ground position and height of selected GCPs. In-situ measured GPS (North, East) coordinates in EPSG 32631 reference system and respective heights.

#	ID	source	screen shot	ground camera shot
1	66004	multipurpose		
2	440002	Voxel		
3	66063	multipurpose		
4	440016	Voxel		

5	440017	Vexel		
6	66021	multipurpose		
7	66065	multipurpose		
8	440021	Vexel		
9	440003	Vexel		
10	66009	multipurpose		
11	440009	Vexel		

<p>12</p>	<p>66026</p>	<p>multipurpose</p>		
<p>13</p>	<p>66043</p>	<p>multipurpose</p>		
<p>14</p>	<p>440019</p>	<p>Vexel</p>		
<p>15</p>	<p>66024</p>	<p>multipurpose</p>		
<p>16</p>	<p>66029</p>	<p>multipurpose</p>		
<p>17</p>	<p>110015</p>	<p>ADS40</p>		
<p>18</p>	<p>66010</p>	<p>multipurpose</p>		

19	66014	multipurpose		
20	440010	Vexel		
21	440014	Vexel		
22	66038	multipurpose		
23	66049	multipurpose		
24	66032	multipurpose		
25	66036	multipurpose		

26	440025	Vexel		
----	--------	-------	--	---

Table 10: ICPs selection over Mausanne site. Similarly to the selection of GCPs (Table 10), ICPs from the same 3 datasets were selected and located on the orthoimagery based on the available visual information (ground camera shots and image screenshots).

A.5 Internal QC by image provider

An in-house QC was operated by Astrium using two sources of points as ICPs for validation:

- the GCPs provided by JRC and used in orthocorrection (#9 per product)
- CPS from Ortho CG13 internal source, derived from aerial photos (#40 in total) and with 15cm resolution over AOI.

The final accuracy of the complete set of ortho-products was checked by one user, in one software environment. The output results of this in-house validation are displayed in Figure 17, and show that Pléiades-1A sensor meets CAP geometry accuracy requirements of $RMSE_{1D} \leq 2.5m$, in accordance with the results of Section 6.3. The Figure 18 represents the sensitivity of the orthocorrection *w.r.t.*:

- the number of GCPs used for a given orientation,

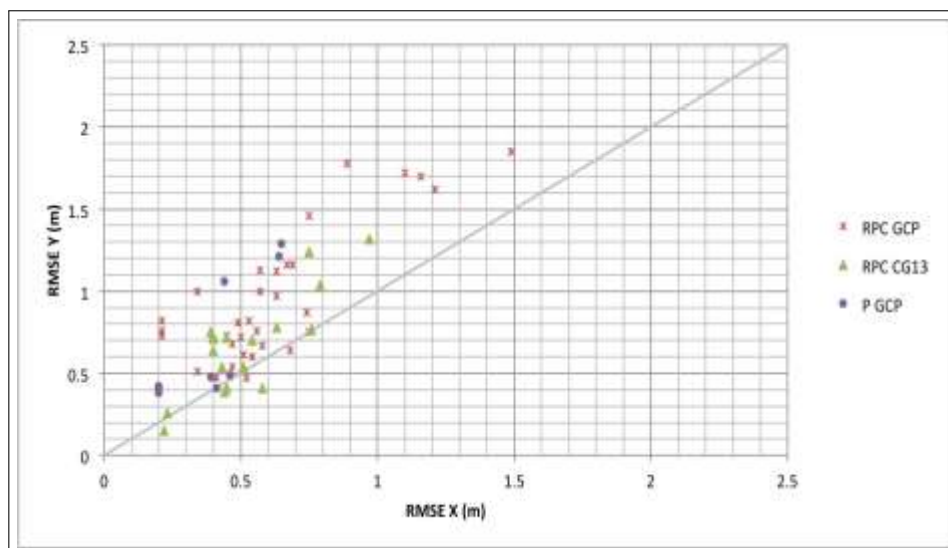


Figure 17: Overall representation of $RMSE_{1D}$ error evaluated by Astrium. Graph of RMSE measurements in Easting/Northing directions over ICPs from Ortho CG13 internal source. Note that the RMSE results are displayed for RPC models evaluated over the input GCPs (red asterisk symbols *) and

Ortho CG13 points (green triangular symbols \blacktriangle), and rigorous models evaluated over the input GCPs only (purple bullet symbols \bullet). See Figure 12 for comparison with JRC EQC results. CAP requirement $RMSE_{1D} \leq 2.5m$ is fulfilled.

- the image viewing angles and
- the mathematical model used for sensor orthorectification,

while evaluating its effect on ortho-image accuracy measured over both GCPs and Ortho CG13 based datasets.

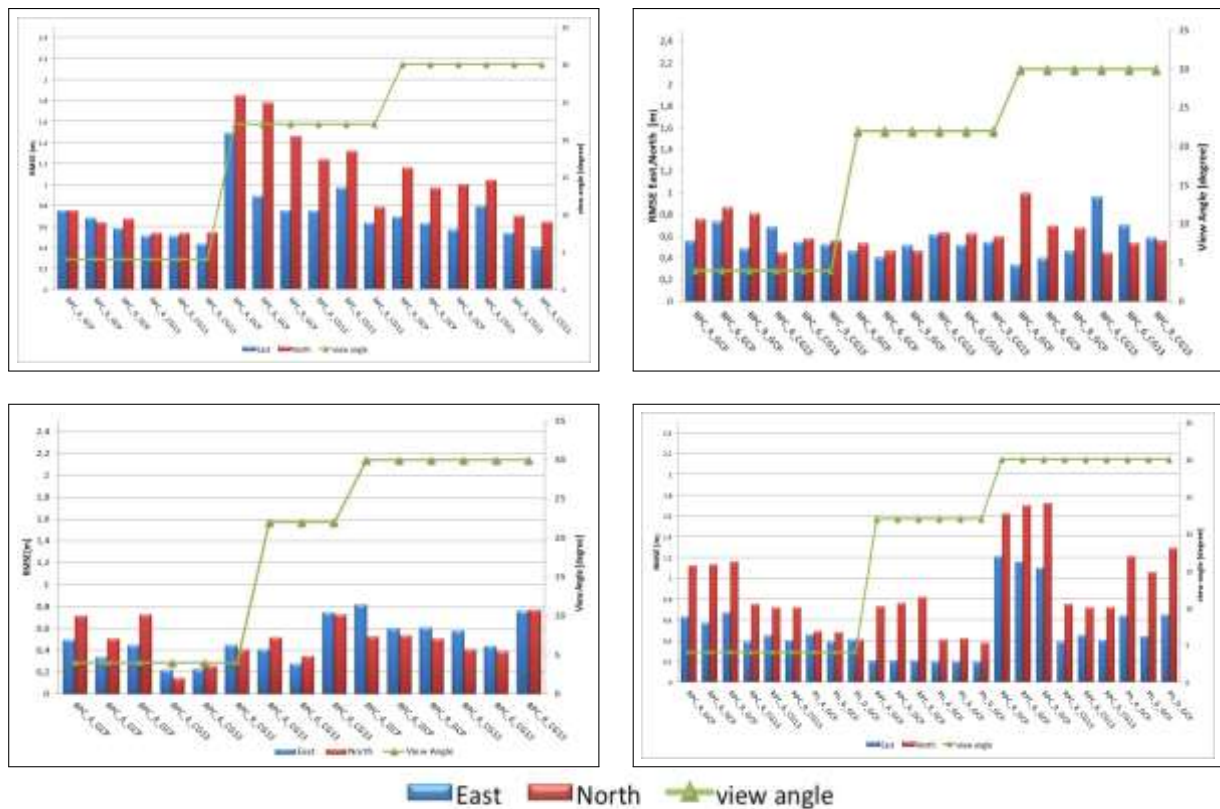


Figure 18: Graph representation of error measured over ICPs from Ortho CG13 Astrium internal source. The RMSE measured over the ortho-rectified products is represented as a function of the number of GCPs used in the orthorectification process for the different software suites and models (RPC and rigorous). From top to bottom, from left to right: the results using PCI, Envi, ERDAS and both RPC and rigorous PixelFactory resp. are presented. For each one of those softwares, both East and North errors (in blue and red resp.) for all 4°, 22° and 30° images (green steps) are displayed. Note the syntax: e.g. RPC 4 GCP stands for the geometric evaluation over Ortho CG13 points of the orthoproduct based on RPC model using 4 GCPs, Ph 4 CG13 stands for the geometric evaluation over the input GCPs of the orthoproduct based on rigorous model using 9 GCPs. See Figure 13 for further description and for comparison with JRC EQC results.

A.6 Additional EQC results representation

The Figures displayed in the following represent the already discussed results of Table 3

– $RMSE_{1D}$ in Easting and Northing directions, but $RMSE_{2D}$ as well – so as to show the sensitivity of the orthorectification outputs *w.r.t* the software suite used for its implementation (Figure 19), the mathematical model used for orthorectification (Figure 20) and the image viewing (off-nadir) angle of the input primary image (Figure 21). These graphs aim at complementing the observations and comments presented in Section 6.3.

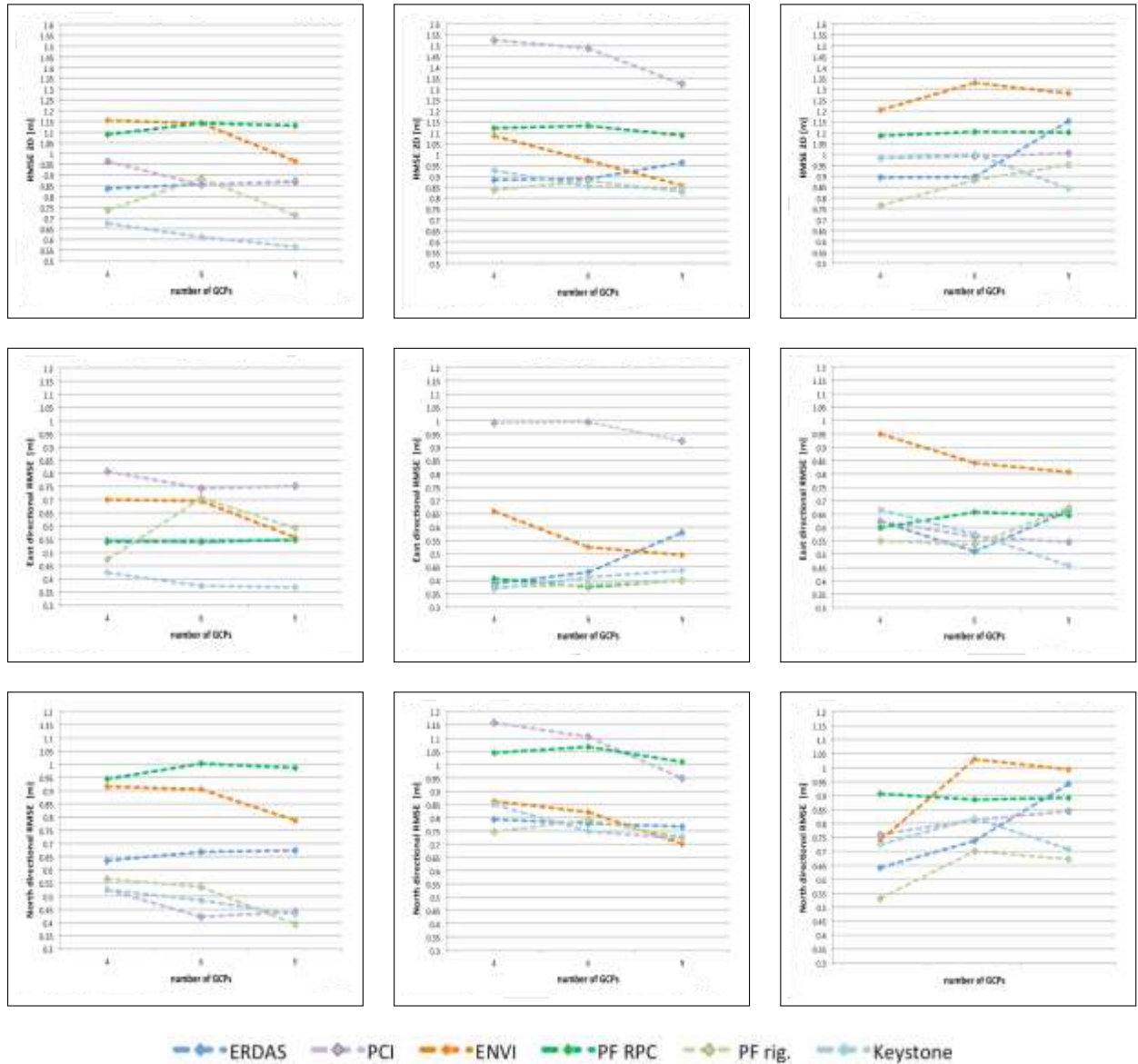
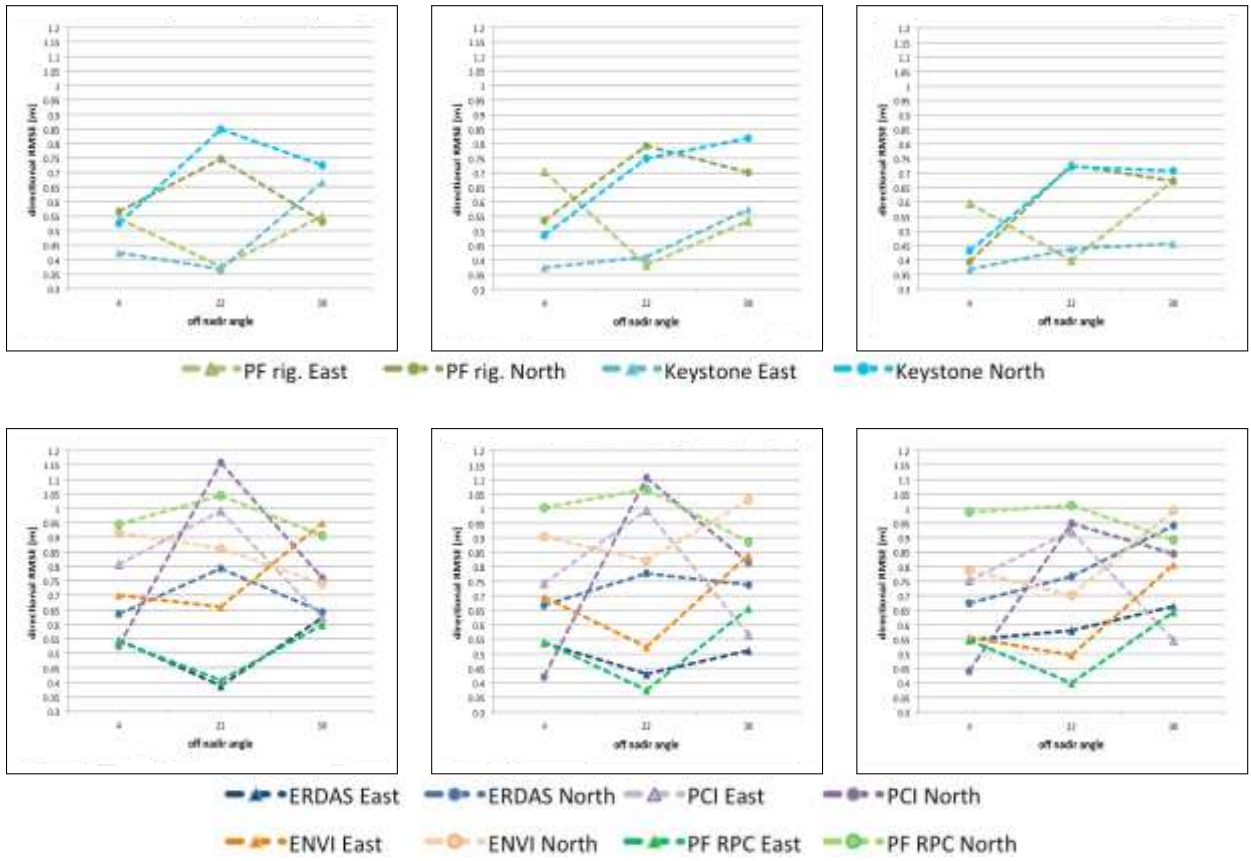


Figure 19: Accuracy sensitivity to software. The output RMSEs are represented for each software suite used in orthorectification as a function of the number of input GCPs (4, 6 and 9 only). From top to bottom: 2D bidirectional error $RMSE_{2D}$, 1D directional errors $RMSE_{1D}$ in Easting and Northing directions resp. From left to right: 4°, 22° and 30°.



#	East	North	2D	#	East	North	2D	#	East	North	2D
rigorous models											
4	0.448	0.5	0.3711	4	0.6079	0.6281	0.8745				
6	0.5395	0.5	0.3971	6	0.5549	0.7594	0.9407				
9	0.4808	0.4	0.418	9	0.5655	0.6898	0.8971				
RPC models											
	40.6488	0.7554	1.0108		40.6112	0.9645	1.1535		40.6982	0.7618	1.0414
	60.6294	0.7493	0.9982		60.5806	0.9427	1.12		60.6434	0.8665	1.0798
	90.6006	0.7226	0.9582		90.599	0.8568	1.0573		90.6651	0.9179	1.1344

Figure 20: Accuracy sensitivity to model. Top graphs: the $RMSE_{1D}$ errors are represented for the different software suites used in the orthorectification process (top: rigorous and bottom: RPC models), as a function of the orientation (off-nadir viewing angle) of the primary image and the number of GCPs (from left to right: 4, 6 and 9) employed. Bottom tables: both $RMSE_{1D}$ and $RMSE_{2D}$ errors are averaged over the different rigorous (top) and RPC models (bottom) models and displayed for the different orientations (from left to right: 4°, 22° and 30°).

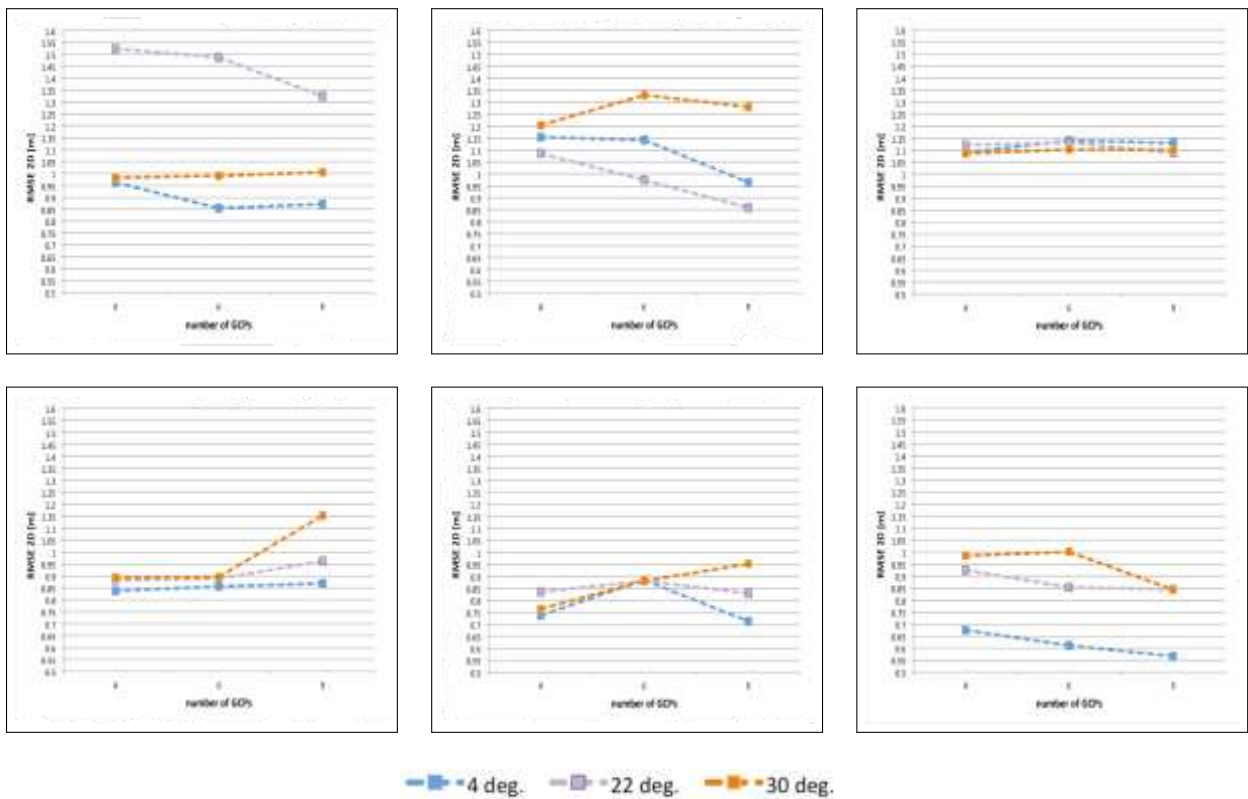


Figure 21: Accuracy sensitivity to viewing angle. The output $RMSE_{1D}$ are represented for all input orientations (off-nadir viewing angles) considered for orthorectification as a function of the number of input GCPs (4, 6 and 9 only). From top to bottom, from left to right: PCI, Envi, PixelFactory RPC, ERDAS, PixelFactory rigorous and Keystone.

References

- [1] JRC IES, *Common technical specifications for the 2012 CwRS campaign*, 2012, available at <http://mars.jrc.ec.europa.eu/mars/content/download/2313/12060/file/CwRS-2.pdf>.
- [2] P.J. Astrand, E. Gervasini, and B. Vajsova, *VHR image acquisition specifications for the CAP controls (CwRS and LPIS QA)*, JRC IPSC, 2011, available at <http://cidportal.jrc.ec.europa.eu/home/sites/default/files/user/documents/13923.pdf>.
- [3] P.J. Astrand, J. Grazzini, F. Ranera, and C. van der Sande, "Validation of Pléiades-1a sensor for use in CAP checks programme - Geometry benchmarking and some CAPI tests", in *Proc. 18th GEOCAP Conference*, 2012.
- [4] J. Nowak Da Costa and A. Walczyn'ska, "Geometric quality testing of the WorldView-2 image data acquired over the JRC Maussane test site using ERDAS LPS, PCI Geomatics and Keystone digital photogrammetry software packages – Initial findings with annex", Tech. Rep. 64624, JRC IPSC, 2011, available at http://publications.jrc.ec.europa.eu/repository/bitstream/111111111/22790/1/jrc60424_lb-nb-24525_en-c_print_ver.pdf.

- [5] P.J. Astrand, M. Bongiorno, M. Crespi, F. Fratarcangeli, J. Nowak Da Costa, F. Pieralice, and A. Walczynska, "The potential of WorldView-2 for ortho-image production within the "Control with Remote Sensing Programme" of the European Commission", *International Journal of Applied Earth Observation and Geoinformation*, vol. 19, pp. 335–347, 2012.
- [6] J.A. Richards and X. Jia, *Remote Sensing Digital Image Analysis – An introduction*, Springer-Verlag, Berlin Heidelberg (Germany), 2006.
- [7] W. Linder, *Digital Photogrammetry – A Practical Course*, Springer, 2009, 3rd edition.
- [8] D. Kapnias, P. Milenov, and S. Kay, "Guidelines for best practice and quality checking of ortho imagery", Tech. Rep. 48904, JRC IPSC, 2008, available at http://mars.jrc.ec.europa.eu/mars/content/download/1231/7140/file/Orthoguidelines_v3_final.pdf; wiki available at http://marswiki.jrc.ec.europa.eu/wikicap/index.php/Guidelines_for_Best_Practice_and_Quality_Checking_of_Ortho_Imagery.
- [9] J.P. Cantou, G. Maillet, D. Flamanc, and H. Buissart, "Preparing the use of Pléiades images for mapping purposes: preliminary assessments at IGN-France", in *Proc. ISPRS - Commission I*, 2006, vol. 36.

References

- [10] S. Baillarin, L. Lebegue, and P. Kubik, "Pléiades-HR system qualification: A focus on ground processing and image products performances, a few months before launch", in *Proc. IEEE IGARSS*, 2009, pp. 76–79.
- [11] S. Baillarin, C. Panem, L. Lebegue, and F. Bignalet-Cazalet, "Pléiades-HR imaging system: ground processing and products performances, few months before launch", in *Proc. ISPRS - Commission VI*, W. Wagner and B. Székely, Eds., 2010, vol. 38, pp. 51–55.
- [12] C. Panem, F. Bignalet-Cazalet, and S. Baillarin, "Pléiades-HR system products performance after in-orbit commissioning phase", in *Proc. ISPRS*, 2012, vol. 39, pp. 567–572.
- [13] C. Latry, S. Fourest, and C. Thiebaut, "Restoration technique for Pléiades-HR panchromatic images", in *Proc. ISPRS*, 2012, vol. 39, pp. 555–560.
- [14] M. Crespi, F. Fratarcangeli, F. Pieralice, A. Walczynska, J. Nowak Da Costa, and P.J. Astrand, "Sensitivity of the WorldView-2 satellite orthoimage horizontal accuracy with respect to sensor orientation method, number and distribution of ground control points, satellite off-nadir angles and strip length", Tech. Rep. 66797, JRC IPSC, 2012, available at http://publications.jrc.ec.europa.eu/repository/bitstream/111111111/26748/1/jrc66797_eur24973.pdf.
- [15] J. Nowak Da Costa and A. Walczynska, "Geometric quality testing of the Kompsat-2 image data acquired over the JRC Maussane test site using ERDAS LPS and PCI Geomatics remote sensing softwares", Tech. Rep. 60285, JRC IPSC, 2010, available at <http://publications.jrc.ec.europa.eu/repository/bitstream/111111111/15039/1/lbna24542enn.pdf>.
- [16] J. Nowak Da Costa and P.A. Tokarczyk, "Maussane test site auxiliary data: existing datasets of the Ground Control Points", Tech. Rep. 56257, JRC IPSC, 2010.
- [17] C. Lucau and J. Nowak Da Costa, "Maussane GPS field campaign: methodology and results", Tech. Rep. 56280, JRC IPSC, 2009, available at http://publications.jrc.ec.europa.eu/repository/bitstream/111111111/14588/1/pubsy_jrc56280_fmp11259_sci-tech_report_cl_jn_mauss-10-2009.pdf.
- [18] T. Toutin, "Geometric processing of remote sensing images: models, algorithms and methods", *International Journal of Remote Sensing*, vol. 10, pp. 1893–1924, 2004.
- [19] M. Crespi, F. Giannone, and D. Poli, "Analysis of rigorous orientation models for pushbroom sensors. Applications with QuickBird", in *Proc. ISPRS - Commission I*, 2006.

- [20] K. Di, R. Ma, and R.X. Li, "Rational functions and potential for rigorous sensor model recovery", *Photogrammetry Engineering and Remote Sensing*, vol. 69, no. 1, 2003.
- [21] J.A. Gutierrez and B.S.R. Armstrong, *Precision Landmark Location for Machine Vision and Photogrammetry – Finding and Achieving the Maximum Possible Accuracy*, Springer-Verlag, London (UK), 2008.
- [22] D. Marr, *Vision: A computational investigation into the human representation and processing of visual information*, W.H. Freeman & Company, San Francisco (USA), 1982.
- [23] JRC IES, *Orthoimage technical specifications for the purpose of LPIS*, wiki available at http://marswiki.jrc.ec.europa.eu/wikicap/index.php/Orthoimage_technical_specifications_for_the_purpose_of_LPIS.
- [24] L. Bunis, "Aerial photography field office – National Agriculture Imagery Program (NAIP) suggested best practices – Final report", Tech. Rep., ITT Space Systems Division, 2007, available at http://www.fsa.usda.gov/Internet/FSA_File/naip_best_practice.pdf.
- [25] J. Grazzini and P.J. Astrand, "External quality control of Pléiades orthoimagery – Part II: Geometric testing and validation of a Pléiades-1B orthoproduct covering Maussane test site", Tech. Rep. 83367, JRC IES, 2013.

List of Figures

1	Benchmarking workflow.	10
2	Maussane test site.	11
3	Pan-sharpened Pléiades acquisitions over Maussane and corresponding foot-prints.	12
4	Example of ground camera shots of GCPs positioning.	14
5	Overall selection of the GCPs over Maussane site and use in ortho products generation.	15
6	GCPs configurations.	16
7	Localisation over the primary images of the GCPs used for orthorectification. .	17
8	Artifact due to the use of a DSM instead of a DTM in the orthorectification. .	19
9	Overall selection of the ICPs used in EQC assessment.	20
10	Identification over the ortho-products of the ICPs used for validation.	21
11	Localisation over the ortho-products of the ICPs used for validation.	22
12	Overall representation of RMSE _{1D} error.	26
13	Graph representation of error measured over ICPs.	27
14	RMSE _{1D} measurements: all software suites, all viewing angles and all GCPs configurations.	28
15	RMSE _{2D} measurements: all software suites, all viewing angles and all GCPs configurations.	29
16	Pan-sharpened Pléiades 16° acquisition over Maussane.	34
17	Overall representation of RMSE _{1D} error evaluated by Astrium.	41
18	Graph representation of error measured over ICPs from Ortho CG13 Astrium internal source.	42
19	Accuracy sensitivity to software.	43
20	Accuracy sensitivity to model.	44
21	Accuracy sensitivity to viewing angle.	45

List of Tables

1	Main characteristics of Pléiades system.	7
2	Benchmarking configurations.	8
3	Planimetric RMSE _{1D} measurements per software suite.	24
4	Planimetric RMSE _{1D} and RMSE _{2D} measurements per orientation.	25
5	Average errors measured over ICPs in orthoimagery products.	26
6	Data quality (DQ) criteria of orthoimage.	32
7	Accuracy of the orthoimagery used in CwRS.	33
8	GCPs selection over Mausanne site.	36
9	Ground position and height of selected GCPs.	36
10	ICPs selection over Mausanne site.	40

European Commission

EUR 26101– Joint Research Centre – Institute for Environment and Sustainability

Title: External quality control of Pleiades orthoimagery – Part I: Geometric benchmarking and validation of Pleiades-1A orthorectified data acquired over Maussane test site

Author(s): J. Grazzini, S. Lemajic and P. Astrand

Luxembourg: Publications Office of the European Union

2013 – 54 pp. – 21.0 x 29.7 cm

EUR – Scientific and Technical Research series – ISSN 1831-9424

ISBN 978-92-79-32538-0

DOI: 10.2788/97660

Abstract

The main objective of the present study is to assess whether Pléiades-1A sensor can be qualified for Control with Remote Sensing (CwRS) programs, specifically in Common Agriculture Policy (CAP) Controls image acquisition campaign. The benchmarking presented herein aims at:

- evaluating the usability of Pléiades-1A for the CAP checks through an estimation of its geometric (positional) accuracy,
- measuring the influence of different factors (angle of view, number of GCPs, orthorectification model) on the abovementioned accuracy.

For that purpose, the External Quality Control of Pléiades-1A orthoimagery conforms to the standard method developed by JRC and follows a procedure already adopted in the validation of previous VHR products.

As the Commission's in-house science service, the Joint Research Centre's mission is to provide EU policies with independent, evidence-based scientific and technical support throughout the whole policy cycle.

Working in close cooperation with policy Directorates-General, the JRC addresses key societal challenges while stimulating innovation through developing new standards, methods and tools, and sharing and transferring its know-how to the Member States and international community.

Key policy areas include: environment and climate change; energy and transport; agriculture and food security; health and consumer protection; information society and digital agenda; safety and security including nuclear; all supported through a cross-cutting and multidisciplinary approach.



Publications Office

ISSN 1775-9279-32538-0



9 789279 325380